Structure and rheology of a physical gel

Moerland, C.P.

Award date:
2014

Technische Universiteit
Eindhoven
University of Technology

Theory of Polymers and Soft Matter
University of Technology Eindhoven

Structure and Rheology of a Physical Gel

Master Thesis

Christian Moerland

Supervised by:
dr. Kees Storm

Final version

Eindhoven, May 20, 2014

Abstract

This report will cover the theory concerning the formation and properties of weak physical gels made out of hydrophobic cores that are linked together with polymer chains. When these molecules are dissolved in water they self organize into cross-linked flowerlike micelles. These gels have a wide range of unique properties and are easy to synthesize with low amounts of material. Having a good physical understanding of the mechanisms that drive the formation of these gels, and how to influence the properties of the gel allows us to do more direct research and produce gels with the desired properties.

Preface

This master thesis found its first inspiration a series of scientific papers by J. van der Gucht and colleagues [1–3] on the formation and the macroscopic properties of a weak physical gel. In the paper they showed that their gel's plateau storage modulus could be described by classical rubber elasticity.

Although the gels made by our colleagues in mechanical engineering (H. Wyss and Z. Fahimi) and simulated using molecular dynamics by H. Mortazavi are in the same category as the ones used by van der Gucht, physical gels, their microscopic structure is completely different. Getting good physical understanding how the macroscopic properties depend on microscopic structure of the molecules is imported in being able to predict and synthesize the desired properties of the gel.

In my master thesis I devoted myself to making a model that has the molecular properties as input and macroscopic properties as output, and in the process getting a understanding of the mechanism that drives the formation of the self-organized structure of these materials.

This would not have been possible without the help and knowledge of the people I worked with, in participially I would like to thank my supervisor Kees Storm for the insightful discussions and guidance that made this report possible. Secondly I would like to thank Hamed Mortazavi with whom I worked in constructing a mesosopic images of the gel. Also I would like to thank our colleagues at mechanical engineering for the useful discussions.

More general I would like to thank everybody that taught me what I know about physics for sharing their knowledge and helping me understand the physics that runs this universe.

Last but not least I would like to thank my parents for supporting me during my study and always being there for me.

Contents

List of Figures

List of Symbols

Table 1: List of used symbols

Symbol	Description
N_0	number of Kuhn segments
a	Length of a Kuhn segment
ν_{eff}	Number of effective cross-linkers
ϵ	Hydrogen bond interaction strength k_bT
n	Number of hydrogen bonds per binder
m	Cluster size
p_l	One binder loop probability
p_b	One binder bridging probability
α	Branching probability
β	Fraction of binders not involved in an infinity chain
G_0	The Flory rubber elastic modulus
Π_0	Osmotic pressure
ρ_m	Number density of clusters in the corona's radius of gyration

Chapter 1

Introduction

A gel is defined as a *Non fluid colloidal network of polymer network that is expanded throughout its whole volume by solvent*[4]. The formation of the gel in the carrier liquid can be characterized as a liquid - solid transition, this process is called gelation. This definition leaves us with a wide range of materials. Because so many materials qualify as a gel we introduce subdivisions in the gel classification. The basic concept stays the same; the elastic modulus is finite and larger than the viscous modulus and it is a colloidal cross-linked polymer network that spans the entire system. A overview of the different types of gels is shown in 1.1[5]. The first distinction we can make by the type of interactions that are dominant in the formation of the gel.

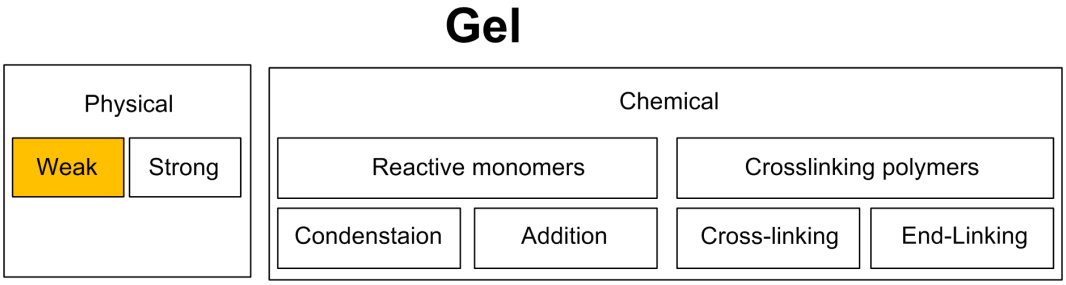

Figure 1.1: Different types of gel ordered by there microscopic properties

The first distinction we make is if the type of interactions of the bonds in the gel are chemical or physical. Chemical bonds are atomic, non reversible, interactions and have a typical interaction energy of a few electron volts (eV). Physical bonds are thermal, reversible, interactions of the order of magnitude of a few k_bT. In the case of the chemical gel we see two different ways of making the atomic bonds in the colloidal network that can be formed by exposure to, e.g. heat, radiation[6,7], reactive monomers and cross-linking polymers[8]. A typical example of a chemical gel is an aerogel shown in figure 1.2 on the left, here the carrier fluid is replaced by a gas after the gel is formed. The result is an ultra lightweight material with very low heat conduction. In the physical regime the bonds are caused by

v/d Waals forces, hydrophobic or electrostatic interactions. Because of this we can control the interactions by changing the pH[9], ionic strength or temperature[10]. In the category of physical gels we define two sub divisions; strong physical gels that have a linear shear modulus up to an deformation of 25% and weak physical gels that are only linear up to an deformation of 5%, but generally have self healing properties. A typical example of a strong physical gel is gelatin shown in figure 1.2 on the right.

Figure 1.2: An aerogel functioning as isolation between a flame and a flower (left). I typical example of a strong physical gel we all know, gelatin (right).

In this report we will focus on weak physical gels, this type of gels are require a relatively low amount of material to synthesize. The properties of the gel can be varied fairly by making changes to the building blocks the gel is made of. This makes that weak physical gels have a wide range properties we can control, leading to a wide range of applications. An example of an application is drug delivery[11] where the gel is injected and slowly dissolves in the body releasing the drug at a controlled rate without the need for intravenous therapy. This means the patient does not have to stay in the hospital for a drip, freeing up valuable bed space. Another group of people that could benefit from this drug delivery system are patients that have having trouble keeping track of their medication. Being able to predict properties like rheology and viscosity, and manipulate them is important here since the gel needs to be able to be injected through a thin needle, yet when in the body it needs to act like a solid where you want to control the release rate of the drug. There are many more application of weak physical gels like wound care[12], tissue engineering materials[13], dental care[14] injectable polymeric systems[15] and other applications like rheology regulation in polymer blends[16]. Because of the versatility of these kind of gels having control over there macroscopic properties and understanding the physical mechanisms that drives these properties is very useful.

In this report we will construct a theoretical framework that predicts the macroscopic properties of the gel depending on the microscopic properties of the building blocks we have control over, like interaction strength and polymer length. We will do this by making a free energy analysis of the microscopic properties and use this to predict the mesoscopic structure

of the gel. This can than be translated to macroscopic properties. The building blocks of the particular gel we model are called “binders” and “linkers”, see figure 1.4 (micro). These binders are stiff rod like particles can form hydrogen bridges with other binders to form clusters, their chemical structure is shown in figure 1.3 on the left. The binders are connected

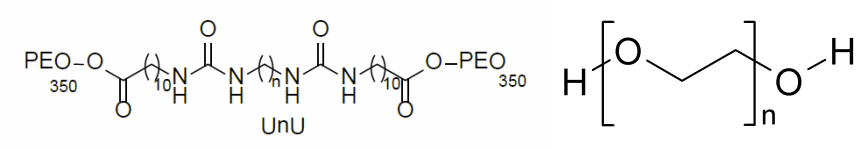

Figure 1.3: Left the chemical structure of the binder and right the chemical structure of the linker (PEG/PEO)

to each other via polymer chains, we will call these chains linkers. We will model these chains as self avoiding Gaussian chains made out of N_0 Kuhn segments, a Kuhn segment is the distance it takes for the directional vector of the polymer chain to be uncorrelated, this length we call a. The linkers are made of polyethylene oxide often referred to as PEG or PEO. The chemical structure of the linkers is shown in figure 1.3 on the on the right. The first step is to define the free energy difference between the different states of aggregation, this we can use to calculate the structure of the clusters. The theory concerning the free energy difference will be covered in section 2.1. Since the binders are interconnected they from a network like structure like shown in figure 1.4 (meso). We can find this mesoscopic structure of the network by using the single cluster’s structure in a mean field approximation. This will be covered in section 2.2. Once we have the average mesoscopic properties we can translate these to macroscopic properties using standard techniques. The techniques concerning the elastic properties of the gel in section 2.3.

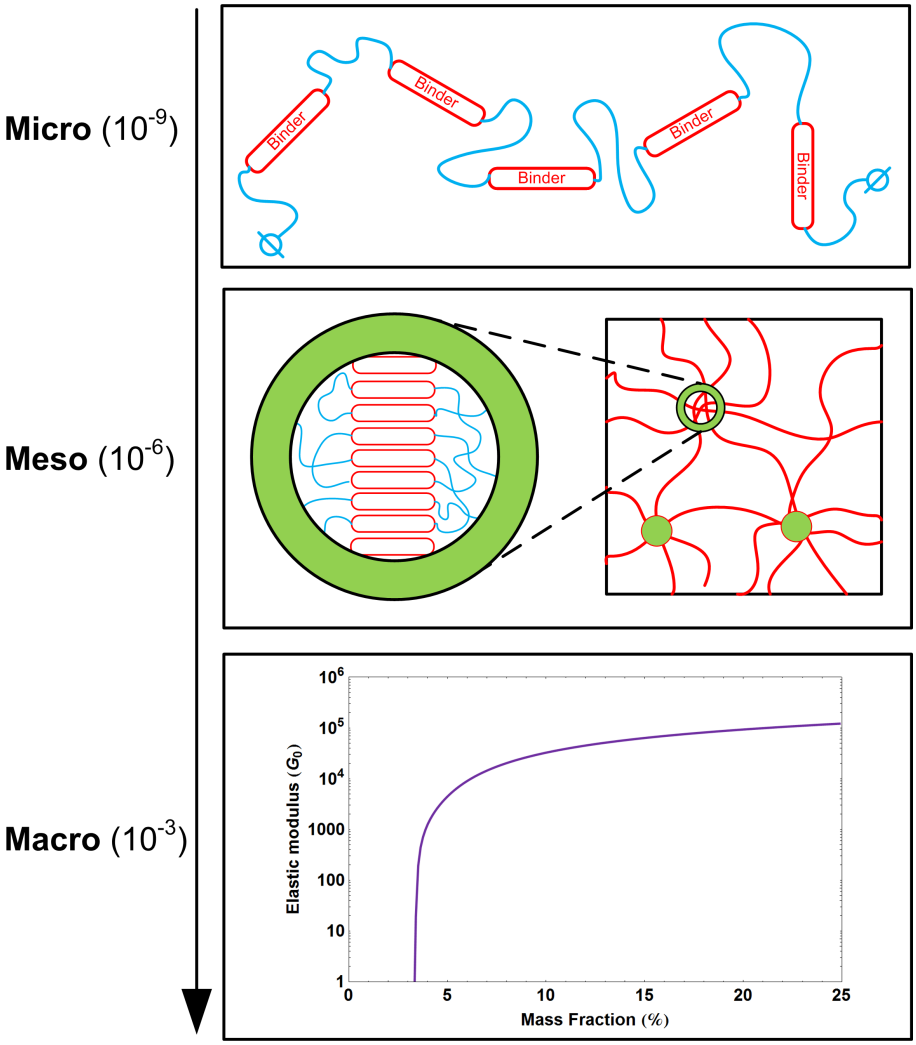

Figure 1.4: The multi scale approach used in the report, starting at molecular interactions and resulting in macroscopic behavior.

Chapter 2

Theory of a Physical Gel

In this chapter we will set up a framework to go from the microscopic parameters of the system, such as energetic interaction strength and the length of the polymer chains, to macroscopic properties that can be measured in experiments like the elastic and viscoses modulus. We will do this by making a free energy analysis of the **microscopic interactions** of the system and see the free energy difference of stacking binders. We will use this to make a predictions of the cluster network **mesoscopic structure**. This we can translate to the **macroscopic properties** of the system.

2.1 Microscopic interactions

In this section we will analyze the free energy difference between lose binders (figure 2.1 left), binder-chains (figure 2.1 middle) and binder-chain cluster (figure 2.1 right). The free energy difference between loose binders and binder-chains we call $\Delta\mathcal{F}_{chain}$, the difference between binder-chains and binder clusters we call $\Delta\mathcal{F}_{cluster}$ for the difference between binder-chains and binder clusters.

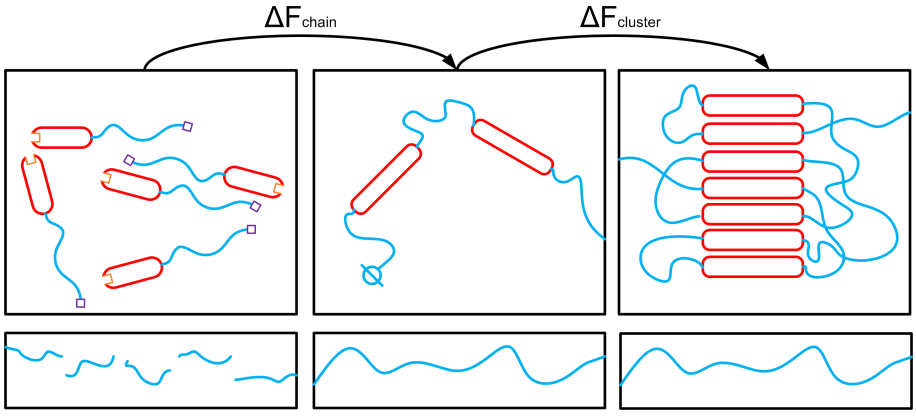

Figure 2.1: Left (1): loose binder-linker units. Middle (2): a unclustered binder-chain. Right (3): a clustered binder-chain.

All the free energies will be per binder, so a cluster with m particles in it will have a free energy difference of $m \times \Delta\mathcal{F}$ where $\Delta\mathcal{F}$ can depend on the cluster size. We find that the free energy difference between a unclustered binder-chain between and a clustered state depends on the number of Kuhn segments in a linker (N_0) the length of a Kuhn segment (a), the interaction strength of the hydrogen bridge (ϵ) in units of k_bT, the number of hydrogen bridges n, the spacing between the clusters ($\delta(m)$) and the cluster size (m)

$$\frac{\Delta\mathcal{F}_{cluster}}{k_bT} \approx -\underbrace{\frac{3\pi(n\times\epsilon)}{5}}_{1} + \underbrace{\frac{3\sqrt{m}}{5}\log\left(\frac{N_0}{\sqrt{m}}\right)}_{2} + \underbrace{\frac{3\delta(m)^2}{2N_0a^2}}_{3} + \underbrace{\frac{2\log(m!)}{m}}_{4}. \tag{2.1}$$

In table 2.1 we list the different components named. In the following sections we will discuss and explain why these terms are here. The free energy difference between loose binders and a binder-chain (both unstacked) is given by:

$$\frac{\Delta\mathcal{F}_{chain}}{k_bT} = -\underbrace{\frac{N_0^{1/5}}{2}}_{5} + \underbrace{\frac{3}{2}\log\left(\frac{3}{2\pi N_0a^2}\right)}_{6}, \tag{2.2}$$

and is caused by the entropy change of the linkers. We treat these terms separately since our colleagues at mechanical engineering use preformed binder-chains to make the gel with.

Table 2.1: The different elements we analyzed for the cluster formation free energy

Number	Description
1	Lennard-Jones rod interaction energy.
2	Corona free energy cost.
3	Entropy cost of making a bridge (stretching the chain).
4	Configuration entropy cost for fixing the linker positions.
5	Self avoidance free energy gain.
6	Chain entropy loss.

2.1.1 Lennard-Jones Rod Interactions

The binders can formed hydrogen bonds, these basically are dipole-dipole interactions and form appendix A.1 we know that the attractive part goes like $1/r^6$, so we model the potential as a simple Lennard-Jones potential

$$\mathcal{U}_{well}(r) = 4\epsilon\left[\left(\frac{b}{r}\right)^{12} - \left(\frac{b}{r}\right)^{6}\right], \tag{2.3}$$

where U_0 the well depth in units of k_bT and r is the intermolecular distance. We model the binders as rods made up out of N individual Lennard-Jones particles with radius b that are stuck together in a rod formation. If we take two parallel infinitely long rods with a small angle between them we can derive the interaction energy as shown in appendix A.2. If we look at the minimum of this interaction energy that is at $r = b$ we find:

$$U_{min} = -\frac{3(n \times \epsilon)\pi}{5}, \tag{2.4}$$

where n is the number of hydrogen bridges and ϵ the strength of a single bond in units of k_bT. We expect to see clusters forming when the bonding energy is equal to, or greater than the entropy cost associated with the formation of the cluster. A single hydrogen bond has a typical strength of around $\epsilon = 1$ to $10k_bT$, the experimentalists use a polymer that has three N-H $\cdots$ O bonds that have a typical strength of $3.3k_bT$ each. The binder is 33 atomic bonds long, assuming that the length of a hydrogen bond is roughly the same as that of a atomic bond we can say that the rod is 33 times longer than the distance between them, this should justify the modeling as if they where infinitely long. The total interaction strength of the binder is thus roughly $19k_bT$.

2.1.2 Corona free energy

The polymer chains in our system are modeled as self avoiding Gaussian chains, this means they are in a swollen state and not ideal, meaning they take up some physical volume. The first order correction to an ideal Gaussian chain are the two particle interactions on the same linker, or excluded volume interactions between the monomers. The gels made in the lab have a chain that has 3 atomic bonds per Kuhn segment, using this we can make an estimate for the excluded volume we find $v = 2\pi(a/6)^2 a$, where a is the length of a Kuhn segment. Using the expressions found in B.2 for the radius of gyration and the free energy cost associated with the self avoidance we find:

$$\langle R_{avoid} \rangle \approx 0.7 a N_0^{3/5}, \tag{2.5}$$

where N_0 is the number of Kuhn segments. For the free energy difference we find:

$$\frac{\mathcal{F}_{avoid}}{k_bT} \approx \frac{N_0^{1/5}}{2}. \tag{2.6}$$

If we start with loose binders and make a binder chain out of them we start the free energy difference for the chain length going to infinity goes to

$$\frac{\Delta\mathcal{F}_{avoid}}{k_bT} \approx -\frac{N_0^{1/5}}{2}. \tag{2.7}$$

Putting in some numbers for a typical linker with 180 Kuhn segments we have an self avoidance free energy gain of proximally $1.4k_bT$. In our system the polymer chains get concentrated

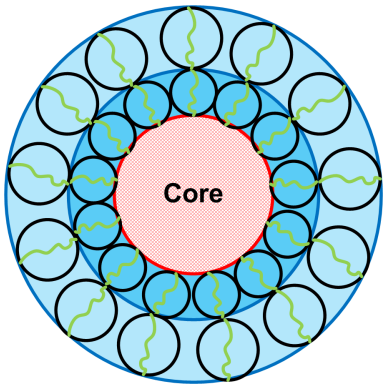

Figure 2.2: A schematic representation of the corona polymer shell around a binder core.

around the clusters core as schematically shown in figure 2.2. This leads to the chains getting in the way of one other and changing their behavior compared to just a self avoiding situations. The polymer chains will not only have a self avoidance but they also start feeling the presence of the other chains. This gives rise to an corona free energy [17] cost per binder of:

$$\begin{aligned} \frac{\Delta\mathcal{F}_{corona}}{k_bT} &\approx \sqrt{m}\log\left(\frac{aN_0^{3/5}m^{1/5}}{a\sqrt{m}}\right), \\ &= \frac{3}{5}\sqrt{m}\log\left(\frac{N_0}{\sqrt{m}}\right), \end{aligned} \tag{2.8}$$

for $N_0 \ll \sqrt{m}$, so long chains, or small clusters. Because of this effect the radius of gyration of a cluster's corona is different than that of a single self avoiding polymer chain,

$$\langle R_{corona}\rangle \approx aN_0^{3/5}m^{1/5}. \tag{2.9}$$

For a typical linker with 180 Kuhn segments and a cluster size of 10 to 20 we find that this corona free energy is roughly 7.7 to 9.9 k_bT.

2.1.3 Entropic Analysis of a Polymer Sol

The last thing we need to look at is the entropy of the linkers and binders before and after the formation of binder-chains and clusters. From expression B.7 we see that the that the entropy of a Gaussian chain depends on R, the end to end distance and N the number of monomers and is given by [18]:

$$S(R) = \frac{3k_b}{2}\log\left(\frac{3}{2\pi N_0 a^2}\right) - \frac{3k_b\vec{R}^2}{2N_0a^2}. \tag{2.10}$$

The difference in free energy between loose binders and a binder-chain is caused only by the linkers between them and is given by:

$$\Delta S_{chain} = -\frac{3k_b}{2} \log\left(\frac{3}{2\pi N_0 a^2}\right), \tag{2.11}$$

per binder. For derivation see appendix B.3. For typical values of N_0 and a we find that this is around $30\mathrm{k_b}T$. If clusters are formed out of the binder-chain we fold the linkers, however it turns out that this does not give rise to an entropy change along as the individual linkers, as well as the chain as a whole, can still be described as an ideal chain (random walk). See appendix B.4 for the derivation.

When we look to the system as a whole we see that forming the cluster we lose configuration entropy,

$$\Delta S_{config} = -\frac{2k_b \ln(m!)}{m}, \tag{2.12}$$

per binder, found via the Boltzmann entropy formula (see appendix B.4 for more details). For some typical values of the cluster size, 10 to 20 we find that this term is 1.5 to $2.1k_bT$.

The last entropic term is that of the difference between if two consecutive binders are in the same cluster (loop) or in different clusters (bridge). Since we assumed that the individual linkers are still behaving as Gaussian chains when they are in the stack we can use the equation B.14 to find the difference between a loop ($R \approx 0$) and a bridge ($R \approx \delta(m)$), where $\delta(m)$ is the inter cluster distance. Doing this we find the entropy cost of making a bridge is:

$$\Delta S_{bridge} = -\frac{3k_b \left(\delta(m)\right)^2}{2N_0 a^2}, \tag{2.13}$$

and zero for a loop. Which is between 1 and $100k_bT$.

2.2 Mesoscopic Structure

In order to say something about the rheology we will need to say something about the structure of the gel. We will do this by computing the probability a cluster increases in size by using the free energy differences found in section 2.1. The size of the clusters, and their configuration can be used to predict the mesoscopic structure of the gel.

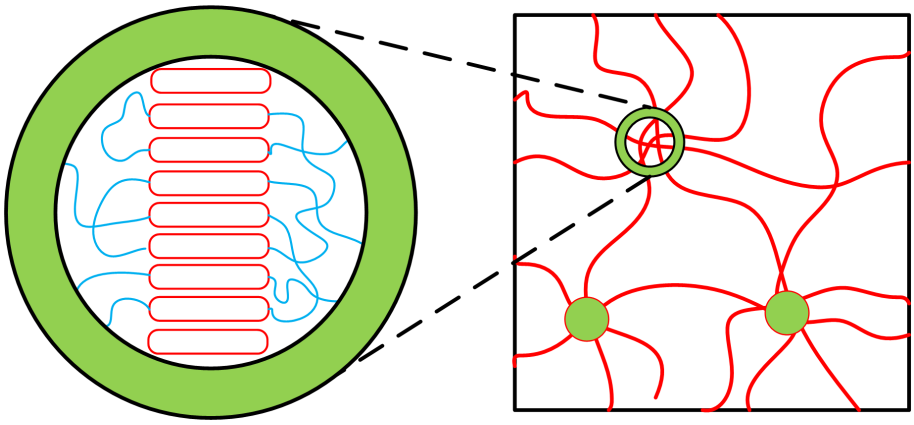

Figure 2.3: The binders form stacks that are interconnected resulting in a network structure of polymer chains.

2.2.1 Looping and Bridging probability

Our system consists of a fixed number of binders N a volume V and the temperature T, so canonical. The N binders in the system can make clusters. If we look at a single cluster and add a particle to this cluster the free energy of that particle changes with $\Delta\mathcal{F}_{cluster}$ and the cluster size is increased by one. If the particle is not added to this cluster the free energy does not change and the cluster does not increase in size. In the system we want to model we

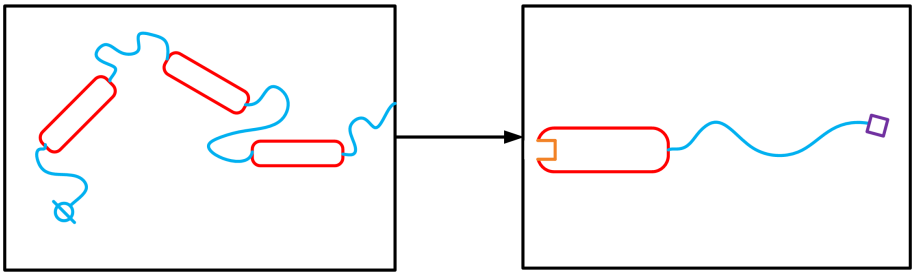

Figure 2.4: Left: A poly chain where the linkers are already connected to the linkers. Right: the building blocks used to model our system. The linkers will link tho one another the chain ends will connect to an other linker in a formed system.

have pre-formed binder-chains as shown in figure 2.4 on the left, these chains have typically 25 elements. In our model we will view the binder-linker chains as loose particles (figure 2.4

on the right), since its easier to compute the statistics per particle. We will omit the extra free energy term, $\Delta\mathcal{F}_{chain}$, that we have since we know the chains are preformed.

The probability the cluster grows in size we call p_+, this can be broke down in to two contributions a loop and a bridge. A loop is where the linker from one binder ends in on the same cluster (figure 2.5 on the left). A bridge is when the linker connects to an binder in an other cluster (figure 2.5 in the middle). In figure 2.5 on the right we see an example of a cluster with four binders in it, one loop and three bridges and three open slots. We will assume that all the clusters are the same, so the three open slots will get filled by three bridges from another cluster. For the probability of looping we know that the end to end

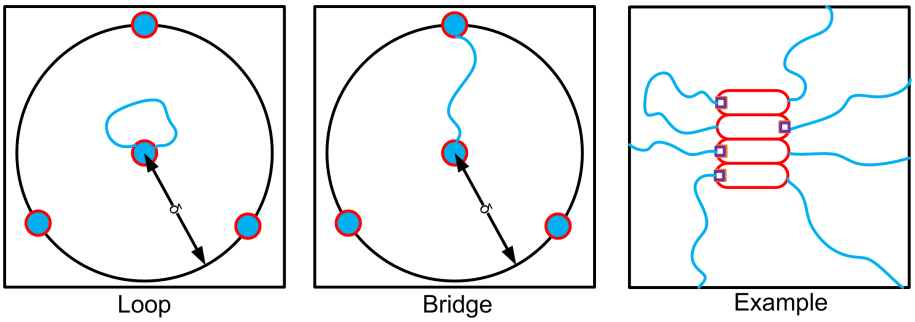

Figure 2.5: A schematic representation of a loop (left), bridge (middle) and a cluster of size $m = 4$ with one loop and three bridges and three acceptation places left (right).

distance, $\vec{r}$, of a linker is small. The probability on a loop is given by the integral over space, but we need to filter out all $\vec{r}$ that are not ending in the same cluster. We will approximate the clusters as point particles, so a loop is when $\vec{r} = 0$.

$$p_{+,l} \approx \int \delta(\vec{r}) p_+(\vec{r}) \mathrm{d}V \sim p_+(0), \tag{2.14}$$

where $\delta(r)$ Dirac delta function functioning as a filter function. The birding probability also goes with $p_+(r)$ integrated over space and only has a finite value if there is an other cluster to bridge to.

$$p_{+,b} \approx \sum_i \int \delta(\vec{r} - \vec{R}_i) p_+(\vec{r}) \mathrm{d}V \sim \rho_m p_+(\delta), \tag{2.15}$$

where we assumed the clusters are spaced equally with a distance δ. ρ_m is the number of clusters any cluster can bridge to. From now on we will not write down the $+$ anymore, so the probability on a loop is given by p_l and on a bridge p_b.

When clusters are formed and grow larger the cluster density goes down assuming they keep using all the available space. This causes the entropy cost for a bridge to scale with m as schematically shown in the figure 2.6. The avarage number of clusters we can make bridges to, ρ_m can be found by looking at how many clusters there are in the corona's radius

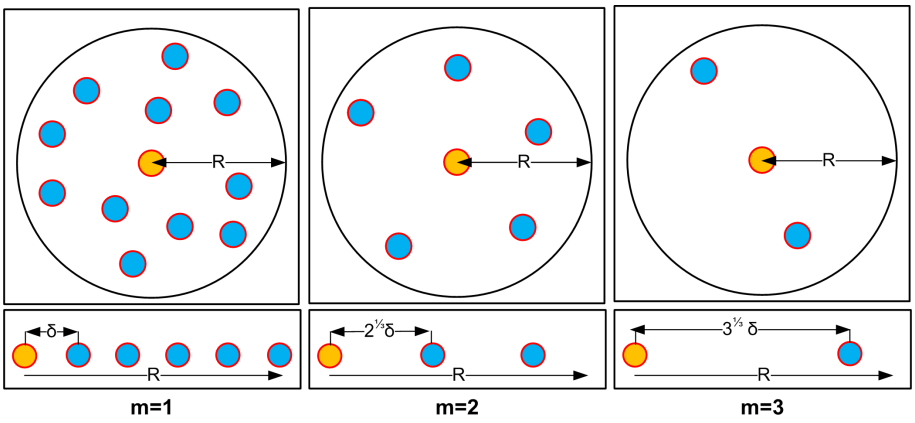

Figure 2.6: A schematic representation of the relation between the cluster size and the cluster spacing.

of gyration $\langle R_{corona} \rangle \approx aN_0^{3/5}m^{1/5}$, the size of the cluster core $m^{1/3}r_{eff}$ and the average distance between the clusters is $\delta = m^{1/3}\delta_0$. We find that the number of clusters we can make bridges to is given by:

$$\rho_m = \left(\frac{aN_0^{3/5}m^{1/5} + m^{1/3}r_{eff}}{m^{1/3}\delta_0} \right)^3 . \tag{2.16}$$

The initial spacing between the binders, δ_0 can be related to the initial density:

$$\rho_0 = \frac{N}{V} = \frac{1}{\delta_0^3}. \tag{2.17}$$

2.2.2 The corona effect

The corona effect is not to be mistaken with the corona free energy. Although both are caused by the dense polymer network around the cluster core, the corona effect is a dynamic limitation to the cluster's growth rather than an energetic. To avoid confusion the dynamic limitation will be referred to as "**the corona effect**" where if we talk about the energetics we will call it "**the corona free energy**". If clusters are formed the network of polymers close to the cluster core gets so dense that a new particle cannot pass the mash of polymer chains surrounding it. This effectively gives us a largest cluster size regardless of the energetic properties of the cluster. To approximate the maximum cluster size we have to calculate how much material there is in the corona, and use this to find a mesh size. We know the corona radius scales with $aN_0^{3/5}m^{1/5}$ and the cluster core takes up mv_0. The total amount of material in the corona it goes as $m \times aN_0$. For the total volume the polymers have at their disposal

we find:

$$\begin{aligned}\frac{3V}{4\pi} &= (aN_0^{3/5}m^{1/5} + m^{1/3}r_{eff})^3 - (m^{1/3}r_{eff})^3, \\ &\approx a^3m^{3/5}N_0^{9/5} + 3a^2m^{11/15}N_0^{6/5}r_{eff} + 3am^{13/15}N_0^{3/5}r_{eff}^2 \end{aligned} \tag{2.18}$$

The mesh of polymer is densest closest to the cluster core, this is because all chains start and end at a cluster core. So we will assume that only the volume given by the last term in equation 2.18 is imported. We will assume that the amount of material in this volume is given by a fraction of the total polymer length we call α_c. α_c is going to be between smaller than 1 and lesser than 0, the typical value we found to give the same results as the gel we try to model is $\alpha_c \approx 1/4$. For the density close to the clusters core we find:

$$\begin{aligned}\rho_1 &= \frac{L}{V}, \\ &\approx \frac{\alpha_c(m \times aN_0)}{3aN_0^{3/5}m^{13/15}r_{eff}^2}, \\ &= \frac{\alpha_c m^{1/3}N_0^{2/5}}{3r_{eff}^2}. \end{aligned} \tag{2.19}$$

This we can use to find a mesh size, $\xi \sim \rho_1^{-1/2}$. If the mesh size is roughly the same size as the typical size of the binders, r_0, the binders can no longer pass and the cluster will not get larger. This gives us a cutoff point:

$$1 = \frac{\alpha_c m^{1/3}N_0^{2/5}}{3}. \tag{2.20}$$

Solving m,

$$m_{max} \sim \frac{2187\sqrt{3}}{\alpha_c^{15/2}N_0^3} \tag{2.21}$$

So, our cutoff function is a function of m and m_{max} where it has to be one for $m \ll m_{max}$ and zero for $m \gg m_{max}$. We also assume that the transition is smooth, so no step function at $m = m_{max}$, but rather a transition zone whose width depends on the interaction energy of the binders. Using these limits we will pick a cutoff function with has these properties:

$$f(m, m_{max}) = \left(e^{\frac{m-m_{max}}{\xi(n\times\epsilon_0)}} + 1\right)^{-1}, \tag{2.22}$$

where ξ determents the width of the function. To match the experimental results we need to set $\xi \sim 1/100$. Note that this function has no physical background, but it does have the correct limites.

2.2.3 Effective number of cross-links

In the next chapter we will show that the effective number of cross-links, the number of bridges being part of a infinite network, is the typical value we need for modeling the system. To find the effective number of cross-linkers, ν_{eff}. The first thing we will define is the probability on making a branch, this is defined as the probability a bridge is connected to another bridge,

$$\begin{aligned} \alpha &= \sum_{i=0}^{\infty} \left[\langle P_b \rangle\right]^2 \langle P_l \rangle^i , \\ &\approx \sum_{i=0}^{\infty} \left[\langle P_b \rangle\right]^2 (1 - \langle P_b \rangle)^i, \\ &= p_b. \end{aligned} \tag{2.23}$$

The probability that one of these ends is part of a infinite system and thus making the cluster part of this network is given by

$$(1 - \beta), \tag{2.24}$$

where β is the probability that this bridge is not part of the infinite network. The probability that all of these bridges in the cluster of the infinite network is,

$$(1 - \beta)^f. \tag{2.25}$$

This adds f effective chains to the system. There is also a chance that only $f-1$ of the chains are part of the structure,

$$\beta(1 - \beta)^{f-1}. \tag{2.26}$$

This adds $f - 1$ effective chains to the network. We do not know which of the f chains is not connected so we need to count all the possible options that are unique, there are: $f!/(f-j)!j!$ unique configurations where j the number of unconnected chains. So for the no-loop cluster we find that ν_{eff} goes as:

$$\begin{aligned} \nu_{eff} &\sim \sum_{j=0}^{j<f} \frac{f!(f-j)}{(f-j)!j!} {\beta_f}^j (1 - \beta_f)^{f-j}, \\ &= (1 - \beta) f. \end{aligned} \tag{2.27}$$

The fraction of bridges that are not being a part of a infinite network is given by [19],

$$\beta_{f,1} = 1 - \alpha + \alpha \sum_{x=1}^{\infty} \frac{1-\alpha}{\alpha} \frac{(fx - x)!}{(fx - 2x + 1)!x!} \left[\alpha(1-\alpha)^{f-2}\right]^x, \tag{2.28}$$

where f is the functionality this is equal to the number of bridges in a cluster. Plotted in figure 2.7 is β for different values of f.

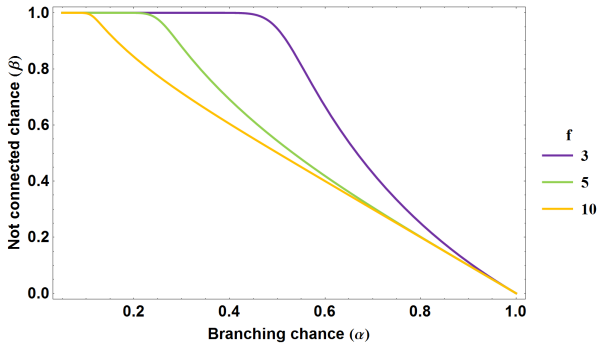

Figure 2.7: A plot of the of β as function of α for different number of iterations (left) and for different values of the functionality (right)

2.3 Macroscopic Properties

In order to translate the mesoscopic structure we found in section 2.2 we will modify some standard technique. The simplest model one can make of a rubber is that of an entangled polymer network made out of ideal polymer chains. In 1953 Flory[18] calculated the the strain-stress relation of a rubber via the entropy change under stress.

2.3.1 Statistics of a classical rubber

In this part we will follow the deviation Flory made to find the modulus of rigidity for a rubber. We start with a long, linear, polymers that are randomly coiled. This is schematically shown on the left side of figure 2.8. When the rubber is formed some of the overlapping polymers will form bonds. This is schematically shown on the right side of figure 2.8. The result is a linear polymer that is now cross-linked on place on fixed points on its contour to other polymer chains[18]. Nodes that connected to a lose end do not contribute the the structures strength,

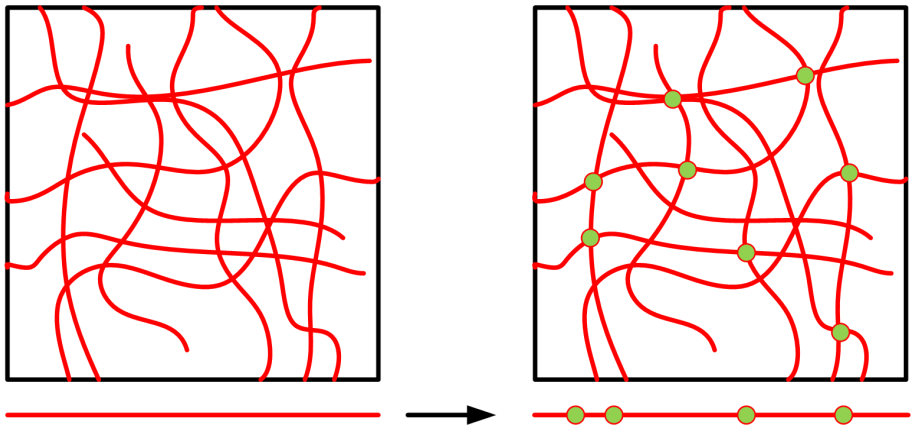

Figure 2.8: Left: A random polymer network. Right: A random polymer network that is fixed together at certain points.

the total number of effective or infrastructural, cross-linkers units is given by the total number of bonds over two (since very bond has two emanating ends in the infrastructural case) minus the number of lose ends[18].

To find the modulus of rigidity we start with a that is structure that is completely formed, so the links are fixed and will not break or change position relative to the polymer chains. Now we put a deformation on the system that is homogeneous throughout the system. So cross-link number i was at position $(x, y, z)_i$ before the deformation and at $(x/a_x, y/a_y, z/a_z)_i$ after the deformation for all i. The magnitude of the deformation is given by a_x, a_y and a_z, these are smaller 1 for stretching and larger than 1 for compression. The number of chains having a specified coordinates (end to end distance) before deformation is given by the probability density function $W(x, y, z)$. Assuming that these nodes distributed according to this function

after a deformation is[18]

$$\nu_i = \frac{\nu W(x_i/a_x, y_i/a_y, z_i/a_z)\Delta x\Delta y\Delta z}{a_x a_y a_z}. \tag{2.29}$$

For a Gaussian chain $W(\vec{r})$ is given by B.7. The next step towards calculating the entropy change concerned with deforming the sample is calculating what the probability of an unlinked network is to be spontaneous in the same state as the deformed linked network. In order to tackle the problem we will assume that we know in advance what ν units of the polymer will be involved in making the links. So we need to find two things so solve the problem:

1. The probability an uncross-linked system will occur, spontaneous, in the same state where the parts designated for cross linking are in the same state as our deformed system.

2. The probability that our predesignated points on the polymer-chain will link.

The first point we can find by using the Gaussian chain distribution density function (see appendix B.1, since every chain's end to end distance is independent of the other chains they factorize. Since it does not matter what chain is where (since we cannot number them) permutation of the chains does not matter for the end result as long as the end result is the same distribution[18].

$$\Omega_1 = \nu! \prod \left(\omega_i^{\nu_i} \nu_i!\right). \tag{2.30}$$

Taking the log, using Stirlings approximation, replacing the sum with an integral and executing the integral we find the first part of the entropy change,

$$k_b \ln(\Omega_1) = -\nu \left[(a_x^2 + a_y^2 + a_z^2 - 3)/2 - \ln(a_x a_y a_z)\right]. \tag{2.31}$$

The second part can be found by the defining the chance that any link is next to an other link within the predesignated volume, δV is $(\nu - 1)\delta V/V$. The chance any off the remaining $\nu - 2$ units is in the same distance from any other of the remaining units is $(\nu - 3)\delta V/V$

$$\begin{aligned} \Omega_2 &= (\nu - 1)(\nu - 3)...(1)(\delta V/V)^{\nu/2} \\ &\approx (\nu/2)!(\delta V/V)^{\nu/2} \end{aligned} \tag{2.32}$$

Now replacing $V \to V a_x a_y a_z$ we find for the second part of the entropy,

$$k_b \ln(\Omega_2) = -(\nu/2)\ln(a_x a_y a_z) + \text{const}. \tag{2.33}$$

Where the constant does not depend on the deformation. If the deformation does not chance the total volume, i.e. $a_x a_y a_z = 1$ the logarithm disappears. In the case where $a_x^2 = 1/a_y = 1/a_z$ we get the following expression for the entropy change under an elongation deformation

is given by:

$$\Delta S = -(k_b \nu_{eff}/2)(a^2 + 2/a - 3) \tag{2.34}$$

where we use the effective number of cross-links ν_{eff} instead of the total number of links ν since the dangling ends to not contribute to the elastic properties of the system. We also replaced a_x by a. We know that the force is given by the gradient in the free energy,

$$f_{orce} = \frac{T}{L_0}\left(\frac{\partial S}{\partial a}\right)_{T,V} \tag{2.35}$$

the stress τ is given by the force per area $f_{orce}L_0/V_0$ and the shear stress γ is $a - 1/a^2$ makes

$$\tau = \left(\frac{\nu_{eff}k_bT}{V}\right)\gamma. \tag{2.36}$$

Where $\left(\frac{\nu_{eff}k_bT}{V}\right)$ is the Flory rubber shear modulus, $G_{0,Rub}$.

2.3.2 Phantom network theory

In our system there are more than two polymer chains emanating form a junction point. The simplest model that takes this change into account is called the **phantom network model**. In this model we replace any branches larger than two emanating form a junction point by one effective new chain. This is done by modeling the junction point with f branches, where the branches are fixed at there end points, schematically shown on the left side of figure 2.9. Making use of a modified end to end distribution function of a Gaussian polymer where the polymer's ends are fixed[5] we find that the new effective length of the polymer chain is given by $K = N/2$, or more general $K = f/2$. Replacing $f - 1$ chains by one effective chain we find that the new length of this chain is given by:

$$N_1 = \frac{N}{f-1}. \tag{2.37}$$

So our node is new connected to the network by:

$$K_1 = N + N_1 = N + \frac{N}{f-1} = N\left(1 + \frac{1}{f-1}\right). \tag{2.38}$$

monomers. This schematically shown on the right side of figure 2.9. If we look at the second of junctions connected to the first one via f^2 chains, shown in figure 2.10 and do the same as for the first generation we find that the number of effective monomers connecting the first node to the network taking two generations into account is given by:

$$N_2 = \frac{K_1}{f-1} = \frac{N}{f-1}\left(1 + \frac{1}{f-1}\right). \tag{2.39}$$

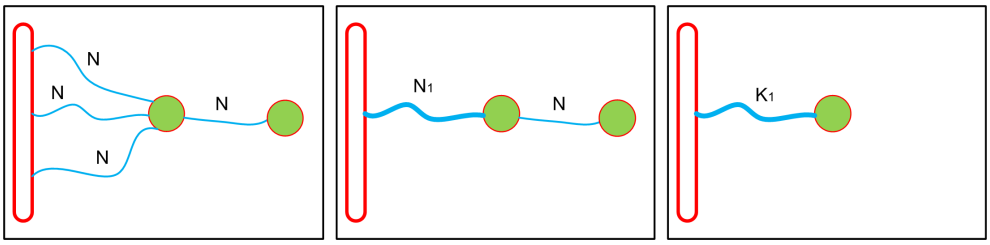

Figure 2.9: (left) A node with functionality $f = 4$ where 3 branches connected to a elastic background and one to another node. (Middle) we replaced the 3 branches with one effective branch. (Right) a single effective branch connecting the node tot the rest of the network.

And the replacement count of monomers for becomes:

$$K_2 = N + N_2 = N\left(1 + \frac{1}{f-1} + \frac{1}{(f-1)^2}\right). \tag{2.40}$$

If we take the number of generations going to infinity we find that the effective number of

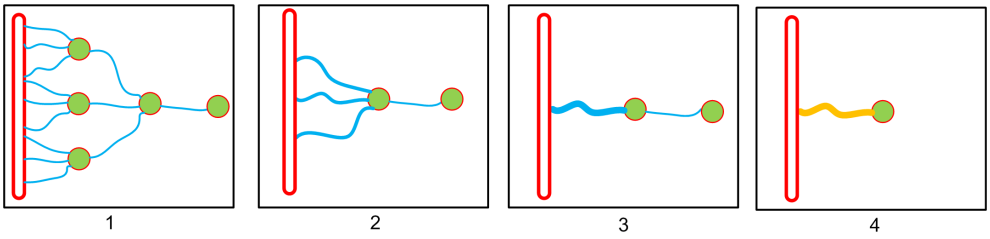

Figure 2.10: (1) The first node connects with 3 branches to other nodes that connect to the elastic background via 3 branches each. (2) Replaced the branches that connect to the effective background by 1 for every branch point. (3) Replaced the 3 effective branches by 1 (4) A single effective branch connecting the node tot the rest of the network.

monomers is given by:

$$\begin{aligned} K &= N\left(1 + \frac{1}{f-1} + \frac{1}{(f-1)^2} + \frac{1}{(f-1)^3} + ...\right). \\ &= \frac{f-1}{f-2}N. \end{aligned} \tag{2.41}$$

We only took one side of the network into account (figure 2.11) where each side is connected by $f-1$ effective chains of length K. If we also take both sides of the network into account we know how many monomers connect the junction to the network.

$$N_{total} = N + \frac{2K}{f-1} = \frac{f}{f-2}N. \tag{2.42}$$

Putting this corrected monomer length into the end to end distribution function B.7 we find

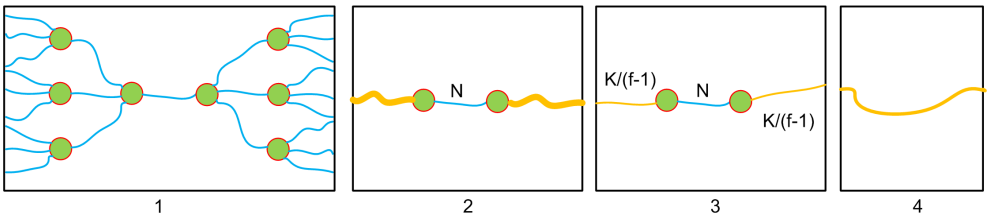

Figure 2.11: (1) The two sides of the network. (2) Replace the two sides by two effective chains. (3) We split the one one link re represent a effective branch. (4) A single replacement branch.

for the elasticity[5]:

$$\tau = \left(\frac{\nu_{eff} k_b T(f-2)}{Vf}\right)\gamma, \tag{2.43}$$

and thus

$$G_{0,Rub} = \frac{\nu_{eff} k_b T(f-2)}{Vf}. \tag{2.44}$$

We will refer to the Flory rubber elastic modulus as G_0.

2.3.3 Osmotic pressure

An other effect that is contributing to the elastic modulus of the system is the osmotic pressure caused by the overlap of aggregates corona's. This overlapping of the corona gives rise to an osmotic pressure. This osmotic pressure can be directly related to the elastic modulus by a pre-factor[20–22] of around 0.01 to 0.001,

$$G_{0,Osm} \sim \Pi. \tag{2.45}$$

A theory linking this pressure to the density of the system is the Alexander[23] - de Gennes[24] model.

$$\Pi(\rho) = \frac{k_b T}{s^3}\left[\left(\frac{V}{V_0}\right)^{\nu_{os}} - \left(\frac{V}{V_0}\right)^{\nu_{el}}\right], \tag{2.46}$$

where s is the mean distance between the anchoring point of the polymers, in our case this can be (experimentally) found by looking at the cluster size and dividing it by the number of linkers in it times two (since every linker has two chains emanating from it). ρ_0 is the density of the blob if it is unperturbed, ρ is the density it has because other clusters corona's are in the way. For neutral particles $\nu_{os} = -9/4$ (shrinking of the system due to crowding effects) and $\nu_{el} = 3/4$ (swelling of the system due to elastic properties of the polymers).

A schematic representation of our system is shown in figure 2.12. L_0 can be estimated by looking at the radius of gyration of a single chain $L_0 \approx a N_0^{3/5} m^{1/5}$. The compressed state can be found by looking at the inter cluster distance, $L \approx m^{1/3}\delta_0$. Since we do not know the

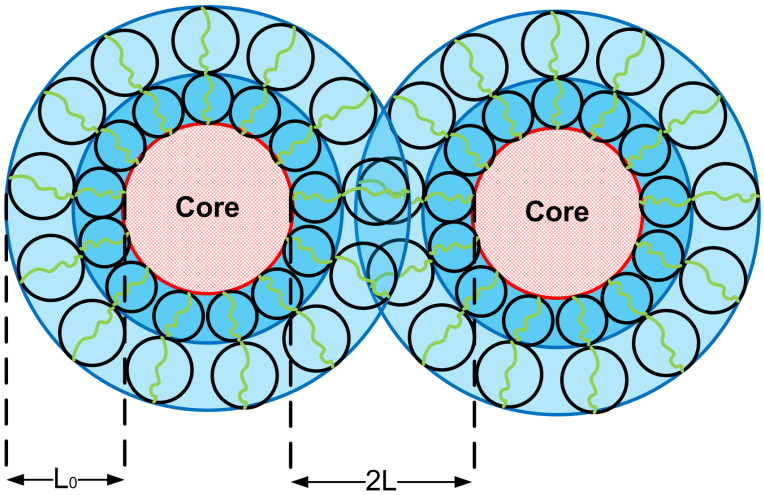

Figure 2.12: An illustration of the system where the corona's of the clusters overlap and cause the local density of chains to go up compared to the native state.

factor between the osmotic pressure and the elastic modulus we will use the osmotic pressure.

Chapter 3

Proof of concept

In this chapter we will show that the theory constructed does gives gives results in the line with experiments and simulations. To do so we first need to is translate the free energy difference shown in figure 3.1 to a probability on finding the different clusters states.

$$\frac{\Delta\mathcal{F}_{cluster}}{k_bT} \approx -\underbrace{\frac{3\pi(n\times\epsilon)}{5}}_{1} + \underbrace{\frac{3\sqrt{m}}{5}\log\left(\frac{N_0}{\sqrt{m}}\right)}_{2} + \underbrace{\frac{3\delta(m)^2}{2N_0a^2}}_{3} + \underbrace{\frac{2\log(m!)}{m}}_{4}. \tag{3.1}$$

First we define two different events for the clusters, it grows and makes a loop or it grown and

Table 3.1: The different elements we analyzed for the cluster formation free energy

Number	Description
1	Lennard-Jones rod interaction energy.
2	Corona free energy cost.
3	Entropy cost of making a bridge (stenching the chain).
4	Configuration entropy cost for fixing the linker positions.

makes a bridge. Assuming we can use Boltzmann statistics to find the relative probabilities we find:

$$p_l(m=1,\vec{r}=0) \sim 1, \tag{3.2}$$
$$p_b(m=1,\vec{r}=\delta) \sim 0, \tag{3.3}$$
$$p_l(m>1,\vec{r}=0) \sim f_m e^{-\Delta\mathcal{F}_l}, \tag{3.4}$$
$$p_b(m>1,\vec{r}=\delta) \sim f_m\rho_m e^{-\Delta\mathcal{F}_b}. \tag{3.5}$$

The free energy difference $\Delta\mathcal{F}$ is given by 2.1 where for a loop we use $\delta(m) = 0$ and for a bridge we use the average cluster distance, $\delta(m) = \sqrt[3]{m}(\delta_0 - r_{eff})$. If we assume the probabilities are independent they factorize, the average number of interactions becomes

(cluster size):

$$\langle m \rangle = \frac{1}{\mathcal{Z}} \sum_{m=1}^{\infty} m(p_l + p_b)^m, \tag{3.6}$$

where we can cutoff the sum for large $m \ll m_{max}$ because of the corona effect (dynamic). The bridging probability of a cluster of size m is given by the sum of all the terms in $\langle m \rangle$ times the number of bridges that terms has times the number of realizations that combination of p_b and p_l. The average number of bridges is given by:

$$\begin{aligned} \langle m_b \rangle &\approx \frac{1}{\mathcal{Z}} \sum_{m=1}^{\infty} \sum_{i=0}^{m} (m-i) \frac{m!}{(m-i)!i!} p_b^{m-i} p_l^i, \\ &= \frac{1}{\mathcal{Z}} \sum_{m=1}^{\infty} m p_b (p_b + p_l)^{m-1}. \end{aligned} \tag{3.7}$$

For the normalization constant we find:

$$\mathcal{Z} = \sum_{m} (p_b + p_l)^m. \tag{3.8}$$

These expressions will gives us the cluster size and the number of bridges a cluster has. The next step is to find what part of these bridges is part of a infinite network since only these cross-links are contributing to the systems strength. If we use equation 2.28 where f is equal to two times $\langle m_b \rangle$. We shown that in our case α is equal to p_b (see equation 2.23), but instead of calculating this we can also use the cluster size and the number of bridges since the probability on a bridge is given by the fraction of bridges in a cluster,

$$\alpha = \frac{\langle m_b \rangle}{\langle m \rangle}. \tag{3.9}$$

In order for the theory to represent the computer simulations or experiments we need to set the constants to the appropriate value. All the used constants used and typical values are shown in table 3.2. The size and mass of the binders and linkers comes form the data the experimentalist supplied, we also used this as an indication for the size and mass for the simulation constants.

3.1 The model and computer simulations

We will try compare the results we find with the results found in the computer simulations. In the computer simulations the binders are modeled as three spheres that interact using a full Lennard-Jones potential with strength ϵ. These LJ-Spheres are linked together by stiff springs and not allowed to rotate relative to one another (red spheres in figure 3.1). The

Table 3.2: Used constants to emulate the computer simulations or the experiments in the model.

What	Symbol	Simulation	Experiment
Binder Length	L_b	5.03×10^{-9} m	5.45×10^{-9} m
Binder Radius	R_b	1.68×10^{-9} m	1.65×10^{-10} m
Binder Mass	M_b	8.70×10^{-22} kg	8.70×10^{-22} kg
Kuhn segment Length	L_k	1.68×10^{-9} m	5.03×10^{-10} m
Kuhn segment Radius	R_k	6.70×10^{-10} m	1.68×10^{-10} m
Kuhn segment Mass	M_k	2.46×10^{-22} kg	7.39×10^{-23} kg
Typical interaction strength	ϵ	1 to 5 k_bT	3.3 k_bT
Number of hydrogen bridges	n	3	3
Typical number of Kuhn segments	N_0	10	180
Corona effect strength	α_c	0.91/0.87/0.81	1/5
Witdh of the cut off function	ξ	$1/100\frac{1}{k_bT}$	$1/100\frac{1}{k_bT}$

polymer chains are also modeled by spring linked spheres, however these spheres are allowed to rotate relative to one another (Blue spheres in figure 3.1). The blue spheres only have the repulsive part of the the Lennard-Jones potential, there connecting springs are tuned so that the radius of gyration is that same as that of an self avoiding polymer chains.

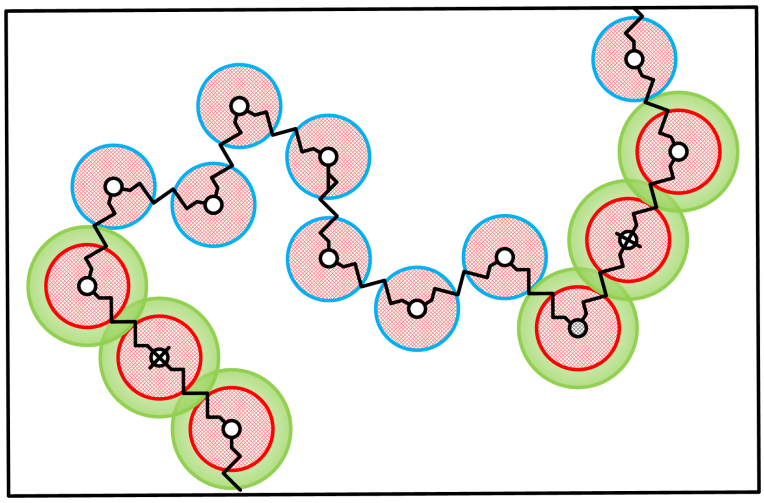

Figure 3.1: An image of the model used to represent the molecules in the computer simulations, the red spheres make up the binder rod and the blue spheres the polymer chains.

In order to match the results found in the computer simulations we set the Kuhn segment length (a) to be the center to center distance, by doing this the number of Kuhn segments (N_0) is the same as the number of beads in the chain. However this is tricky because of the limit $\sqrt{m} \ll N_0$, and the number of beads is small. In the computer simulations there

are very few Kuhn segments meaning we run into this limit rather fast. In addition to this the part of the corona causing the corona effect (dynamic) is close to one for short chains and dropping rather quickly for longer chains so α_c could not be taken constant. The total interaction energy of the rods in the simulations cannot be modeled as that of an infinitely long rod, we found that the interaction energy is roughly 4.5 times ϵ. The parameters used to the computer simulations are shown in table 3.2. The solid line is the result found using

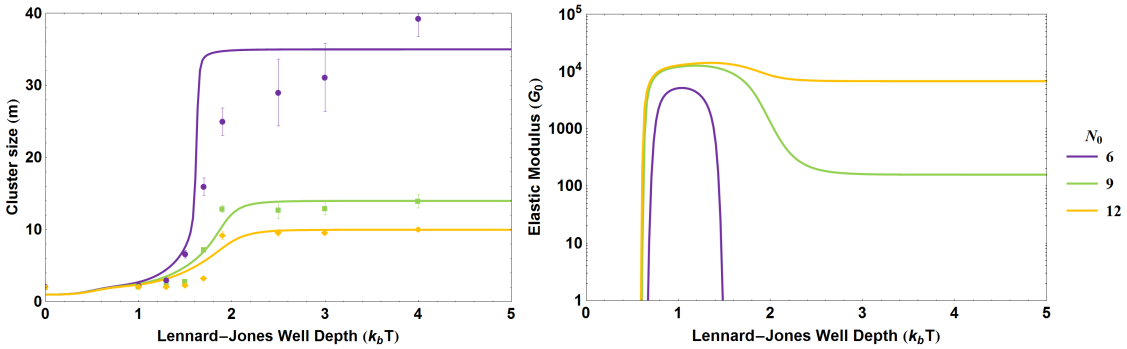

Figure 3.2: A plot of the average cluster size and the cluster (left), the solid line the results found by the theory and the points fount by simulation and the elastic modulus (right) for a mass fraction of 2%

the theory, the dots are the results found using the computer simulations. We see that for the longer chains ($N_0 = 9$ and 12) we are doing pretty close to the simulation results. But for the shortest chain $N_0 = 6$ we see a larger errors and a different trend for $\epsilon > 3$. This is because the theory breaks down here, since the square root of the cluster size is roughly the same as the number of Kuhn segments.

The elastic modulus is also calculated in the simulations using a similar Flory rubber theory and shows the same trends, like higher an elastic modulus for longer chains and the plateau getting wider. However since the elastic modulus depends directly on the density of the system fittings these two plots is impossible at this time. Even though we are at the limit of what the model can predict it still able to produce reasonable results for the cluster size. It is safe to assume that the model does better in the regime of the experimentalists.

3.2 The model and Experiments

For the gel made in the experiments use we do not have the problem of running into the limit $r_0\sqrt{m} \ll aN_0$, where r_0 is roughly the same size as a. Longer chains also means smaller clusters due to the corona effect and corona free energy. Plotted in figure 3.3 (right) is the elastic modulus found using the modified Flory rubber theory and the same values for the constants as the experimentalist used, see table 3.2. The red dots are the actual results from the experiments. Even though the Florry rubber model is one of the simplest model it already is predicting the elastic modulus. Plotting the elasticity as function of the density we can also

see where the percolation points is, since if the network is percolating it will gets a finite elastic modulus. A reason that the Flory rubber theory is not predicting the elasticity correctly is

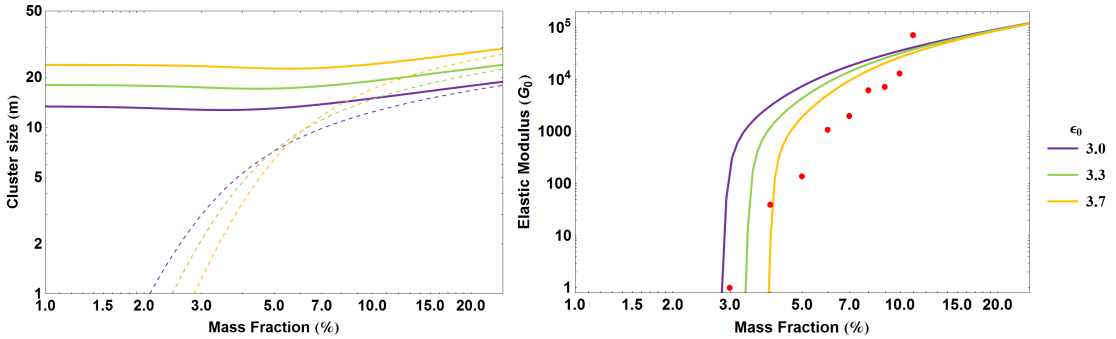

Figure 3.3: A plot of the cluster size (solid) and the number of bridges (dashed) are shown on the left. The elastic modulus is plotted on the right, the solid line the results found by the theory and the points fount by experiments for a chain length of $N_0 = 180$.

that it assumes that the polymers that are getting cross-linked are in a unperturbed state. Where in our case they are getting compressed due to the corona around the clusters core. The next step is to explore the phase space and try to construct a phase diagram.

Chapter 4

Phase Space Exploration

In this section we will discus the results found by the theory and see what the the behavior in terms of cluster size (m), number of effective links (ν_{eff}) and the elastic properties due to cross-linking (G_0) and the osmotic pressure (Π_0) are in terms of the interaction energy ($n \times \epsilon$), spacer (N_0) length and density (ρ_0). For the constants we will use some typical values in the same range as use in the experiments, these variables are shown in table 3.2, the only thing we changed was the corona effect strength ($\alpha_c = 1/4$ instead of $1/5$) to keep the maximum cluster size smaller. We will follow the same structure as the theory starting at the microscopic level and working up to the macroscopic properties.

4.1 Microscopic Interaction

In this section we will use the expression found in chapter 2 for the cluster size and the number of effective cross-links to get an idea of the clusters structure and macroscopic properties depend on the microscopic parameters like interaction energy and spacer length. Making use of the free energy found in section 2.1 (equation 4.1) we find that the bonding probability (equation 2.14 and 2.15) as function of the interaction energy $n \times \epsilon$, the Kuhn length a number of Kuhn segments N_0 the cluster size m and the spacing $\delta_0(m)$. Plotted in figure 4.2 on the left is the distribution of cluster sizes on the right is the average cluster size as function of the density. If $m = 1$, so no loop or bridge is made (nothing happens), we set $\Delta\mathcal{F} = 0$, if $m > 1$ the free energy difference per particle is given by 4.1.

$$\frac{\Delta\mathcal{F}}{k_b T} \approx \underbrace{-\frac{3\pi(n \times \epsilon)}{5}}_{1} + \underbrace{\frac{3\sqrt{m}}{5} \log\left(\frac{N_0}{\sqrt{m}}\right)}_{2} + \underbrace{\frac{3\delta(m)^2}{2N_0 a^2}}_{3} + \underbrace{\frac{2\log(m!)}{m}}_{4}. \tag{4.1}$$

In figure 4.1 (left) we see that increasing the interaction energy (ϵ) increases the free energy gain per particle this causes the energy gain per particle to stay larger (and posetive) for larger clusters. We also see that the maximum gain, per particle, is at $m = 2$ and that in

Table 4.1: The different elements we analyzed.

Number	Description
1	Lennard-Jones rod interaction energy.
2	Corona free energy cost.
3	Entropy cost of making a bridge (stenching the chain).
4	Configuration entropy cost for fixing the linker positions.

becomes lower for larger clusters. In figure 4.1 (right) we see the total cluster energy. We see that the cluster's total energy does has an optimum where the gain per particle is a decreasing function of the cluster size. For systems with a large energy gain per particle we expect to see larger clusters.

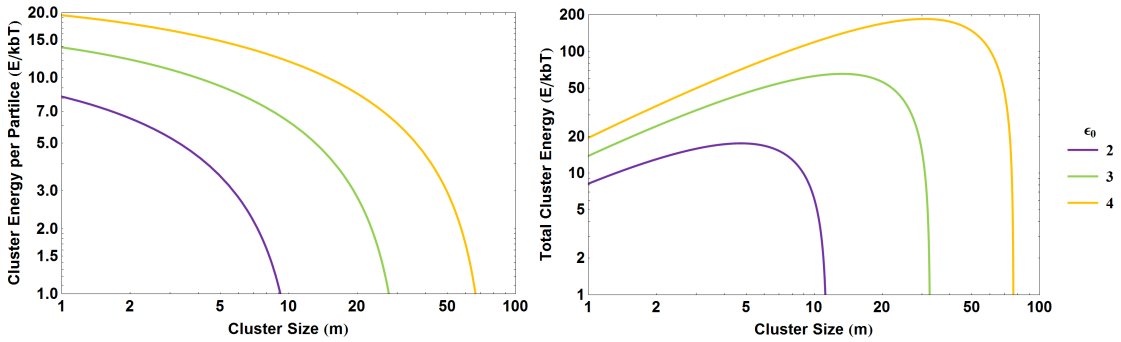

Figure 4.1: A plot of the interaction free energy per particle (left) and for the total cluster (right) for a cluster that only has loops, $a = 5.025 \times 10^{-10} m$, $N_0 = 180$, , $r_0 = 5.445 \times 10^{-9} m$, **a mass percentage of** 3% **and three hydrogen bonds.**

4.2 Mesoscopic Structure

We can use the free energy difference and the probability for increase the cluster size to predict the cluster size and bridge distribution. From this we can calculate the average values using a computer, since the functions cannot be solved analytically without making an approximation for the the $\log(m!)$ term. The probability that the cluster increases in size is given by equation 2.14 and 2.15 we can use these to find the probability that the cluster increases in size:

$$P(m) = \frac{1}{\mathcal{Z}}(p_l + p_b)^m. \tag{4.2}$$

Plotting this for different values of the interaction energy ϵ is shown in figure 4.2. If we

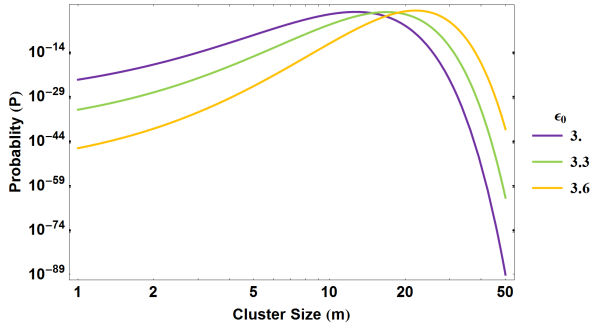

Figure 4.2: A plot of the cluster size distribution as function of the cluster size. The solid line is the cluster size and the dashed line the bridging probablity. $a = 5.025 \times 10^{-10}m$**,** $r_0 = 5.445 \times 10^{-9}m$**, a mass percentage of** 3% **and three hydrogen bonds.**

compare this to the results found using simulations on a similar system by V. Hugouvieux and colleagues[25] we see a similar shape but they also see that the probability of small clusters does go up. This could be caused by dynamic limitations where small clusters get trapped between larger clusters. This we will not be able to see in this theory because of the mean-field approximation.

4.2.1 Mesoscopic structure as function of the Interaction energy

The first thing we will analyze is the cluster size and the number of bridges as function of the binder interaction energy ϵ. In figure 4.3 we plot the cluster size ($\langle m \rangle$ on the left solid line), number of bridges ($\langle m_b \rangle$ on the left dotted line) and number of effective cross-links (ν_{eff} on the right) as function of ϵ for different values of the chain length (N_0). In figure 4.5 we plotted we plotted the same but for different values of the mass fraction (ρ_m) If we look at the cluster size in figure 4.3 we see that we get larger clusters for shorter chains, this is because the corona effect is less strong for short chains. We also see that shorter chains start forming clusters at lower energies than longer chains, this is because the corona free energy

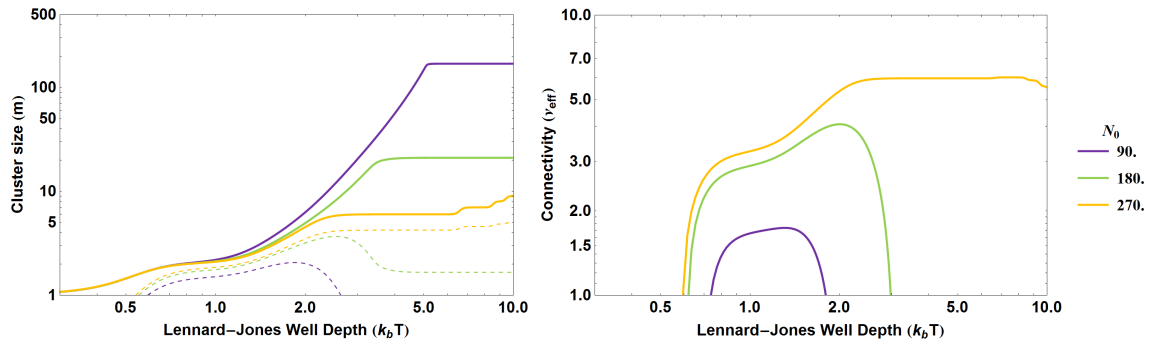

Figure 4.3: A plot of the average cluster size (left) and the number of effective links (right) as function of the interaction energy where $a = 5.025 \times 10^{-10}m$, $r_0 = 5.445 \times 10^{-9}m$, a mass fraction of 3% and three hydrogen bonds.

is per binder is smaller for shorter chains. For all three chain lengths we can define three regimes in the cluster size:

1. The interaction energy is so low no clusters are formed.

2. Clusters start forming and we see strong growth of the cluster size for increasing ϵ.

3. The size of the clusters is constant because of the corona effect (dynamic).

In figure 4.4 we see the visualizations of a system in state two (left) and three (right) made by H. Mortazavi using molecular dynamics simulations. For the connectivity we see that there

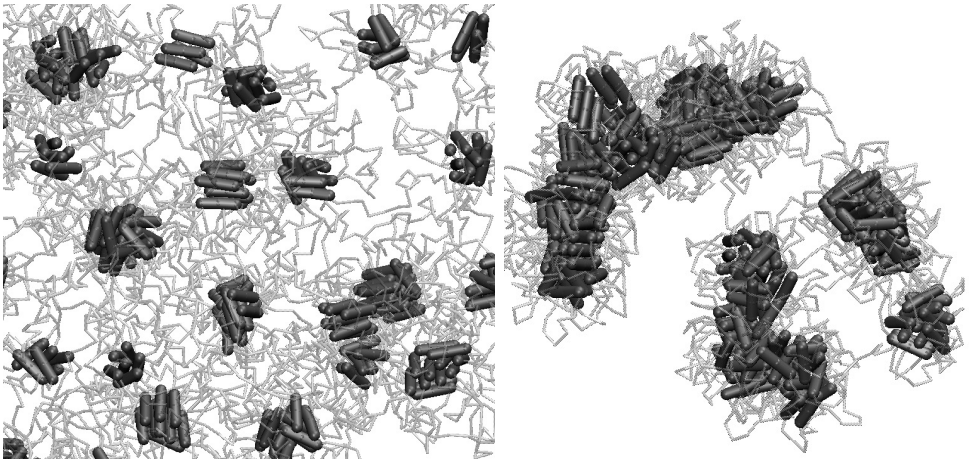

Figure 4.4: A visualization of the states found in molecular dynamics computer simulation. Left a cross-linked state in phase two and right a cross-linked state in phase three.

are no connections if clusters are not formed due to low interaction potentials, this is what we expect logically. It goes down again for high values of the interaction energy, this is because we are getting large, isolated clusters that are not able to interconnect anymore because they

are too far apart from another. These trends are also found in molecular dynamic simulations of the same system.

Making the same plots for a fixed linker length but chancing the starting density of the system (figure 4.5) we see that the clusters start forming at lower interaction strength for higher concentrations. For the connectivity we see that for the low density we get into the regime of large isolated clusters but if the concentration is high enough the clusters keep forming cross-links, even for high interactions strengths. These trends cannot be observed

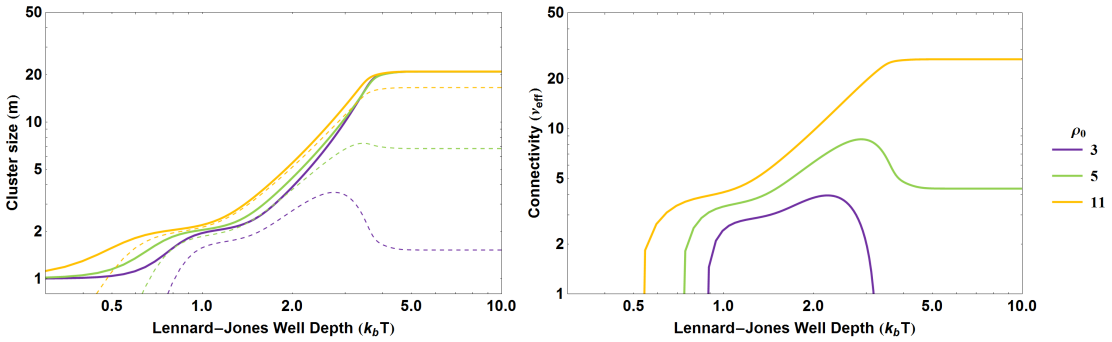

Figure 4.5: A plot of the average cluster size (left) and the number of effective links (right) as function of the interaction energy where $a = 5.025 \times 10^{-10}m$, $r_0 = 5.445 \times 10^{-9}m$, $N_0 = 180$ and three hydrogen bonds.

in simulations because increasing the density gives problems with the periodic boundary conditions.

4.2.2 Mesoscopic structure as function of the Density

From the previous paragraph we know where to put the interaction energy to be in the different regimes. We will focus on the chain length of 180 to start with, so regime one is from 0 to 1, two is from 2 to 4 and three for the interaction energy larger than 5. Plotted in figure 4.6 is the average cluster size (solid line) and the functionality (dotted line) one cluster has as function of the density. From figure 4.6 we see that if we are in regime three density does not matter for the cluster size. We also see that smaller cluster form connections at lower densities. The maximum number of connections per cluster is, off course, limited by the cluster size itself. This means that the absolute value of the connectivity does not directly say anything about the rheology of the system, for this we need to look at the cross-link density. We will do this in the next chapter, for now we will focus on the cluster size and the trends we can see depending on the different values. For experimentalist the easiest thing to change is the density and/or the spacer length. A plot of the cluster size and connectivity as function of the density for different spacer lengths is shown in figure 4.7 for ϵ is 3.3. This means we are in regime two for the spacer length of 90 and 180, where we see that the cluster size does increase if we increase the density. For the spacer length of 270 we are in regime

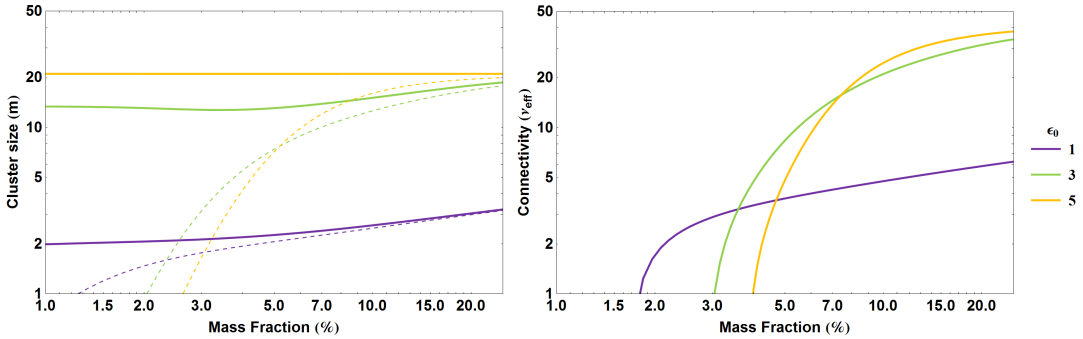

Figure 4.6: A plot of the average cluster size (left) and the number of effective links (right) as function of the density where $a = 5.025 \times 10^{-10}m$, $N_0 = 180$, $r_0 = 5.445 \times 10^{-9}m$. and three hydrogen bonds.

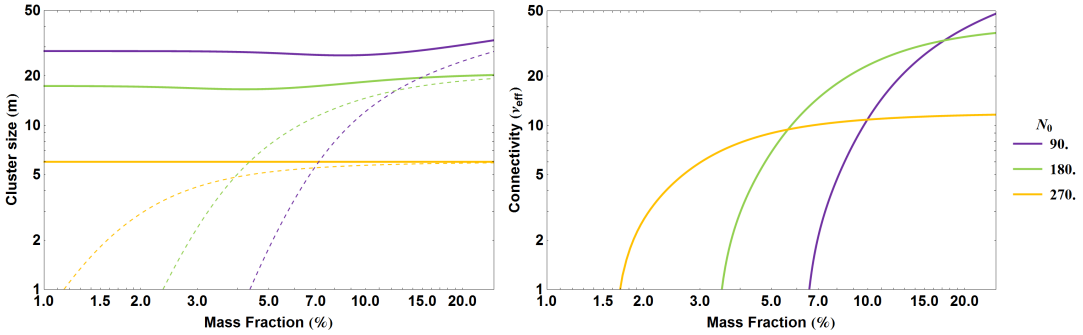

Figure 4.7: A plot of the average cluster size (left) and the number of effective links (right) as function of the density where $a = 5.025 \times 10^{-10}m$, $r_0 = 5.445 \times 10^{-9}m$, $\epsilon_0 = 3.3k_bT$ and three hydrogen bonds.

three. We see that the cluster size does not increase if we increase the concentration, since the corona effect is the limiting factor and does not depend on the concentrations. We also see that longer chains make cross-links at lower concentrations.

4.2.3 Mesoscopic structure as function of the spacer length

So far we seen that the longer chain it start to percolate at lower densities and form smaller clusters at the same mass percentage of material and interaction strength. Plotting the cluster size and connectivity for different number of Kuhn segments. For very short linkers we will be going to regime three, clusters limited in size due to the corona effect. Since smaller chains also means larger clusters we will see the connectivity go down because we are getting large isolated clusters that are too far apart for cross-linking. The point where we go into regime three depends on the interaction energy, for lower interaction energies the point where the corona effect is the limiting factor (regime three) is at sorter chains. Because of the limitation, $N_0 >> \sqrt{m}$ we cannot plot for very short chains lengths.

If the chain length is increased we enter regime two, if it is increased more we enter regime

three again but now there will still be cross-links since we have small cluster cores. In figure 4.8 the red dashed line is the maximum cluster size caused by the corona effect. If we are to the left of this line we are in regime one or two depending on the interaction energy. If we are on the line we are in regime three. Having a long linker also means that the amount of material causing the screening to go down, but here we set it to a constant. However for extremely long linkers we expect small or no clusters, due to the corona free energy. We see

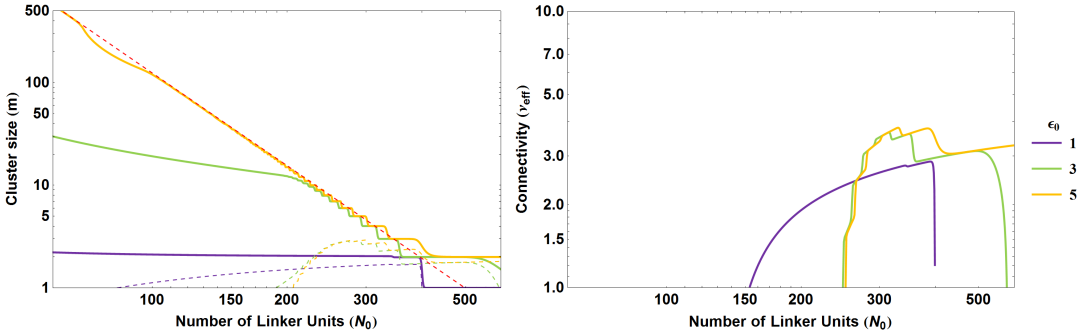

Figure 4.8: A plot of the average cluster size (left) and the number of effective links (right) as function of the density where $a = 5.025 \times 10^{-10}m$, $r_0 = 5.445 \times 10^{-9}m$, a mass fraction of 3% and three hydrogen bonds.

again that small interaction energies lead to small cores, also we see that for increasing the linker length we get smaller clusters. If the linkers are too long we see that no clusters are formed anymore and that there are no cross-links. This happens at shorted chains for lower interaction energies.

The step-like structure indicates the clusters are small. This is a discretization effect in the averaging, caused by the fact that a cluster can only have a whole number of particles (m is an integer) in there core. The average itself does not have to be an integer.

4.3 Macroscopic Properties

In this chapter we will use the mesoscopic structure fount via the microscopic properties to try and predict the macroscopic behavior elastic behavior of the system. For the elastic properties we have two contritions, one is the elastic modulus found via the Flory rubber theory,

$$G_0 = \frac{\nu_{eff} k_b T (f-2)}{V f}. \tag{4.3}$$

The other contribution is the the osmotic pressure that scales linear with the elastic modulus $G_{0,Osm} \sim \Pi_0$ and is given by,

$$\Pi(\rho) = \frac{k_b T}{s^3}\left[\left(\frac{V}{V_0}\right)^{\nu_{os}} - \left(\frac{V}{V_0}\right)^{\nu_{el}}\right], \tag{4.4}$$

We will compare the Flory rubber modulus and osmotic pressure as function of the interaction energy (section 4.3.1), density (section 4.3.2) and linker length (section 4.3.3). We will try to find and explain trends that can be used to make a distinguishing between the two effects.

4.3.1 Macroscopic Properties as function of the Interaction energy

In figure 4.9 on the left we see the same trending behavior as in the simulations, longer chains result in a larger plateau. We also see a maximum just after the gelation point, we also see that the maximum is largest for a chain length $N_0 = 180$. The osmotic pressure as a finite value even before the clusters start cross-linking, see figure 4.9 (right). It is not likely that the system has a finite elastic modulus even before the system is cross-linked, because when a force is exerted on the material the clusters (or loose binders) can just relocate in the carrier fluid. Plotting the curves like this does not show trends we can use to make distinguish between the two effects.

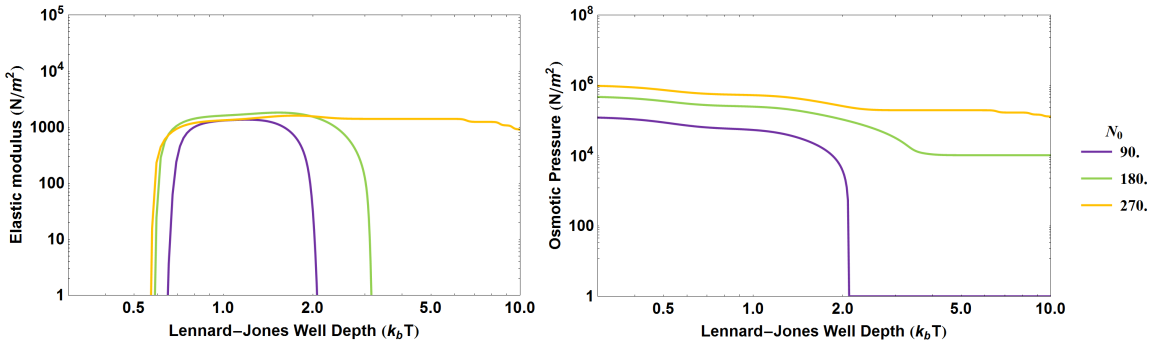

Figure 4.9: A plot of the Flory rubber modulus (left) osmotic pressure (right) as function of the interaction energy where $a = 5.025 \times 10^{-10} m$, $r_0 = 5.445 \times 10^{-9} m$, three hydrogen bonds and a mass fraction of 3%.

4.3.2 Macroscopic Properties as function of the Density

In figure 4.10 and 4.11 we see that the elastic modulus (left) and the osmotic pressure (right) as function of the mass fraction of material used plotted as the solid line. The dashed lines are fits to the plateau modulus. We see that more material yields higher values of the elastic modulus and osmotic pressure. This causes all the slopes of the fits to be positive as shown in table 4.2. In figure 4.10 (left) we see that higher interaction energy causes the system to cross-link at higher densities. On the right in figure 4.10 we see that the osmotic pressure

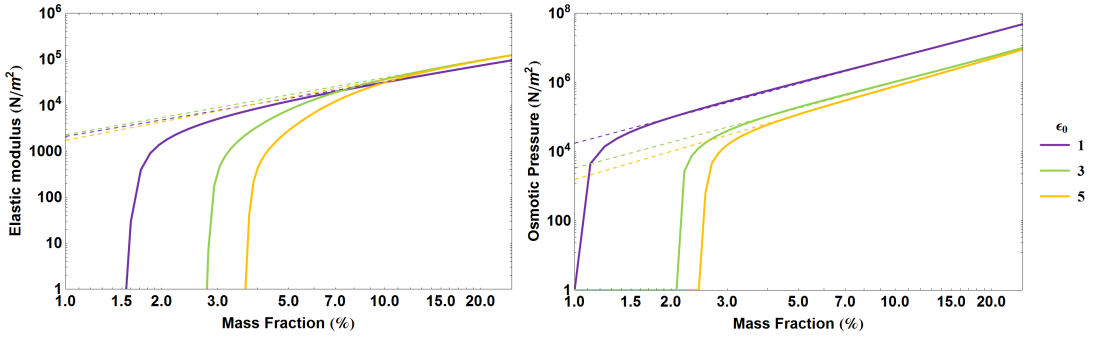

Figure 4.10: A plot of the Flory rubber modulus (left) osmotic pressure (right) as function of the density where $a = 5.025 \times 10^{-10}m$, $N_0 = 180$, $r_0 = 5.445 \times 10^{-9}m$ and three hydrogen bonds

becomes finite at lower densities. Both effects can be explained with the cluster size, lower interaction energies results in smaller clusters and smaller clusters percolate faster since a bridge needs to cover less distance. For the osmotic pressure small clusters mean a higher pressure since the corona scales with $m^{1/5}$ where the distance between he cluster scales with $m^{1/3}$, so

$$\begin{aligned} \Pi(\rho) &\sim \left(\frac{m^{3/5}}{m}\right)^{\nu_{os}} - \left(\frac{m^{3/5}}{m}\right)^{\nu_{el}}, \\ &\approx \frac{1}{m^{9/10}}, \end{aligned} \tag{4.5}$$

so larger clusters means a lower osmotic pressure. If the density is increased the clusters stay small for lower interaction energies, meaning we see the same trend as we see for low densities, lower interaction energy means higher osmotic pressure. For the Flory rubber modulus we find that the number of cross-links a cluster has scales linear with the cluster size. The density also scales linear with the cluster size so we find,

$$\begin{aligned} G_0 &\sim \frac{mp_b}{m\delta^3}, \\ &= \frac{p_b}{\delta^3}. \end{aligned} \tag{4.6}$$

So of the Flory modulus we find that it does not directly depend on the cluster size. Since $p_b \to 1$ for all interaction energies at high concentrations we see that they convent to each other. If we increase the chain length the osmotic pressure also increases (at least if we are

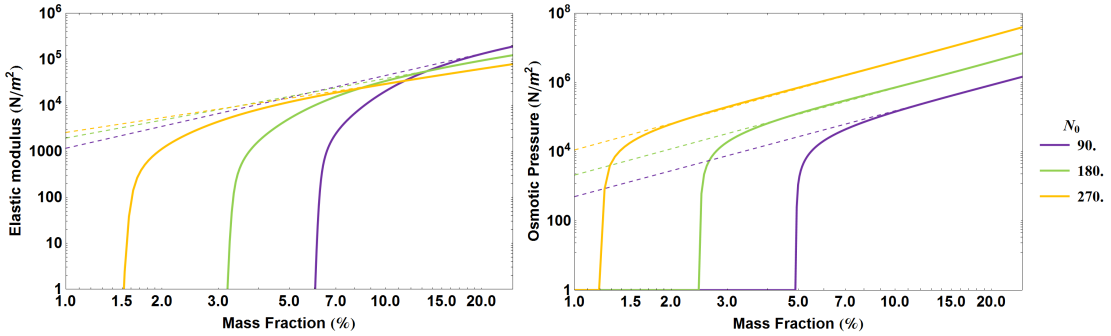

Figure 4.11: A plot of the Flory rubber modulus (left) osmotic pressure (right) as function of the density where $a = 5.025 \times 10^{-10}m$, $r_0 = 5.445 \times 10^{-9}m$, three hydrogen bonds and $\epsilon_0 = 3.3k_bT$ per bond.

in region one or two, so low to moderate interaction energies.), yet the cluster size deceases. Smaller clusters means more cross-links leading to a higher Flory rubber modulus. So, longer chains means a higher Flory rubber modulus but lower osmotic pressure.

In figure 4.11 on the left we see that shorter chains cross-link at higher densities, this has two reasons. One the short chains means larger clusters so a larger cluster to cluster distance and two, the cost of making a bridge is relatively larger since the chain is shorter. If we go to high densities we see that short chains have a slightly higher modulus this is because we are in the regime described by equation 4.6 and $p_b \to 1$, but we are keeping the total mass of used material constant to shorter linkers means effectively more binders. In figure 4.11 on the right we see shorter linkers means lower osmotic pressure. This is because short chains make smaller coronas ($R_{corona} \sim N_0^{3/5}$) and the clusters are larger.

Table 4.2: The slopes fount by fitting (dashed lines) though the different curves in figures 4.9 (above the line) and 4.10 (under the line)

Bond energy (k_bT)	Chain length (N_0)	Flory rubber (Slope)	Osmotic pressure (Slope)
1	180	1.18	2.46
3	180	1.24	2.48
5	180	1.33	2.68
3.3	90	1.58	2.48
3.3	180	1.29	2.51
3.3	270	1.06	2.54

In table 4.2 we see see the slopes of the Flory rubber elasticity and osmotic pressure

depending on the density (so not the cluster size). We see that we have a decreasing slope for increasing linker for the Flory rubber and an increasing slope longer chains if we look at the osmotic pressure. This effect could be used to determine what effect, cross-linking or osmotic pressure is the dominant factor in the elastic response. However in the next paragraph we will see that plotting the Flory rubber modulus and osmotic pressure as function of the linker length and keeping the interaction energy constant gives an easier to recolonize trend.

4.3.3 Macroscopic Properties as function of the linker length

In figure 4.12 we plotted the Flory modulus (left) and Osmotic pressure (right) as function of the linker length for different values of the concentration and keeping the interaction strength constant. The sigh of the slope has a different sign, negative (decreasing) as function of the linker length for the Flory rubber and positive (increasing) for the osmotic pressure (see table 4.3)). The Flory modulus decreases for longer chains since longer chains means a lower

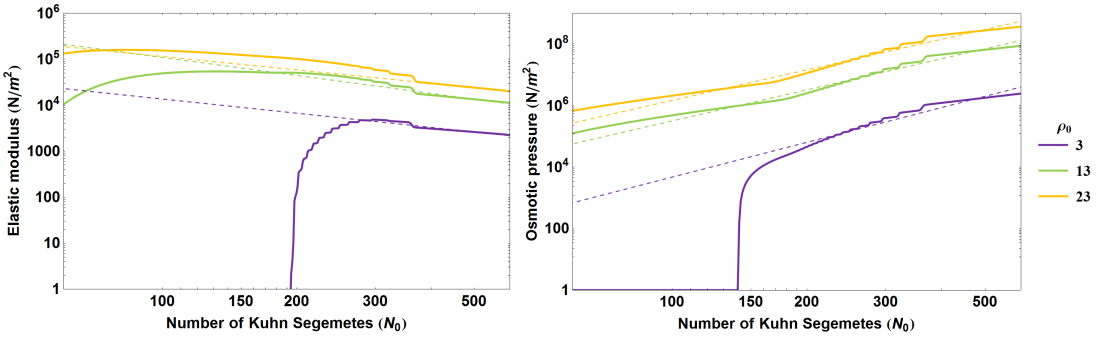

Figure 4.12: A plot of the Flory rubber modulus (left) osmotic pressure (right) as function of the density where $a = 5.025 \times 10^{-10}m$, $r_0 = 5.445 \times 10^{-9}m$, three hydrogen bonds and an interaction energy of $\epsilon_0 = 3.3k_bT$ per bond.

starting concentration. This is because we are keeping the total mass of the material used constant, so longer linkers means less binders for the same mass. So even though the cluster are getting smaller should lead to an increase in the Flory modulus, the spacing between of the clusters is increasing so fast that the number of cross-links per unit volume goes down. The same arguments can be used for the osmotic pressure, smaller cluster leads to higher pressure and less material for a lower pressure. However longer chains also mean larger coronas. The total effect of increasing the linker length for the osmotic pressure is that it increases. The difference in the sign of the slope is probability the easies and most profound to see what effect is dominant in causing the elastic modulus.

Table 4.3: The slopes fount by fitting (dashed lines) though the different curves in figures 4.12

Density (%)	Chain length (N_0)	Flory rubber (Slope)	Osmotic pressure (Slope)
3	180	-1.02	3.76
13	180	-1.3	3.36
23	180	-0.97	3.31

Chapter 5

Results and Conclusion

In this chapter we will discuss the results we found and combine them to form a phase diagram and explain some of observed behavior of the gel. First we will construct a phase diagram of the gel as function of the interaction energy ϵ_0 and linker length N_0, and see how this changes if the density is increased.

5.1 Phase Diagram

In section 4.2.1 we defined three different regimes depending on the interaction energy.

1. The interaction energy is so low no clusters are formed.
2. Clusters start forming and we see strong growth of the cluster size for increasing ϵ.
3. The size of the clusters is constant because of the corona effect (dynamic).

We will start by analyzing the phase diagram at a mass fraction of around 3 percent and start at low interaction energy and keeping this constant and moving from short chains to longer chains. Next will move to higher interaction energies and again start at short chains and move to longer chains. The arrows indicate what would happen if the density is increased.

Blue line The first phase is where there are no clusters formed due to the interaction energy being low. If no clusters are formed the system will not have a elastic modulus. For short chains we see that the percolation starts at higher interaction energies and goes to lower interaction energies if the chain length is increased. This is because the clusters get smaller for longer chains meaning the distance between clusters is smaller, meaning making a bridge cost less energy and thus becomes more likely to happen. For higher densities it also becomes less costly to make the bridges, since the distance between clusters is reduced. Increasing the density means the boundary between phase one and two goes to lower interaction energies. This effect is stronger for short chains. For extremely long chains we see that the point where clusters are formed moves to higher interaction energies, this is because the corona free energy

is larger for long chains. The density has little effect on this point since we just do not see any clusters and the energy it cost to make bridge is already small since the chains are so long. In figure 5.2 the transition point between phase one and two is shown with the blue line.

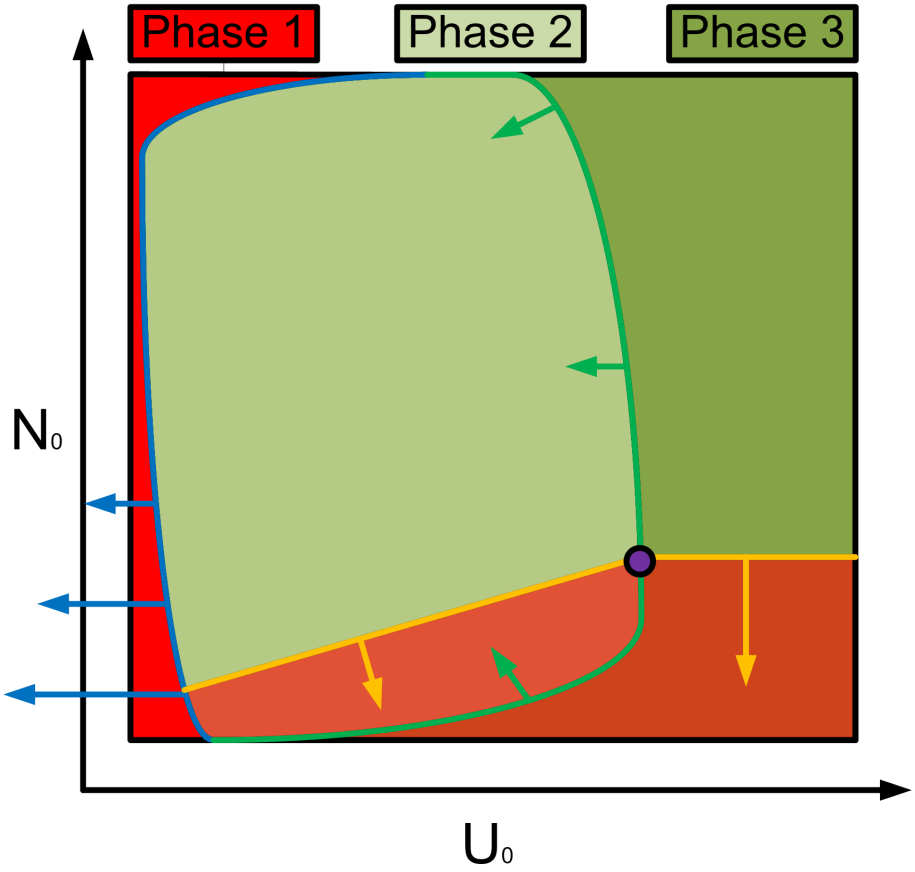

Figure 5.1: A sketch of a phase diagram of a physical gel made out of binder-chains at a moderate density.

Orange line If the interaction energy is increased we see that the clusters grow in size. For short chains these clusters grow fastest because the corona free energy per particle scales with the log of the chain length. The brown area in figure 5.2 is where this effect is so strong that no percolation, these are large isolated clusters. If the density is increased the cluster-cluster distance goes down and the transition from a percolating to a non percolating system is moved to shorted chains. This transition is indicated in figure 5.2 by the orange line and goes down for higher densities. If the chain length is increased the growth in cluster size becomes slower if the interaction energy is increased. This means smaller clusters, thus smaller cluster to cluster distance. The longer chains start forming bridges now and we see percolations.

Green line Moving to even higher interaction energies we see the corona effect kicking in, meaning the cluster size no longer depends strongly on the interaction energy. The transition

between phase two and three is shown in figure 5.2 by the green line. If the density is increased this moves to lower interaction energies, since clusters grow in size is for increasing the density if the system is percolating. For very short chains we move into the regime where the corona effect is dominant for low interaction energies, this is because the cluster grow fast in size due to the corona free energies being small. If we increase the chain length we see clusters grow slower for increasing interaction energy, causing them the reach the point where the corona effect is dominant at higher interaction energies. For even longer chains the maximum cluster size goes down fast, at some point this effect becomes stronger than the slowing of the cluster growth and we see that we reach phase three for lower interaction energies.

Purple point The point where we get large isolated cluster happens at higher interaction energies for longer chains because the clusters grow slower, causing a smaller cluster-cluster distance and it cost less to make a bridge for longer chains. This is why the orange line to move to longer chains for higher interaction energies. When we get to the transition between phase two and three the clusters stop growing as function of the interaction energy. So from the purple point, where the orange and green line cross the percolation point stops depending on the interaction energy and only depends on the linker length and density.

In short Longer chains means the clusters grow slower and are smaller, which causes the connectivity per binder to go up for longer chains. Since we keep the total used mass constant using longer chains also means less binders per unit volume. Increasing the interaction energy causes the clusters to be larger and the connectivity per binder to go down but the bonding energy per unit volume goes up. This scaling stops when we reach the regime where the corona effect is dominant. The maximum in the elastic modulus is expect to be just to the right of the blue line, since the clusters are smallest here. Small clusters mean that the birding probability is large, since the cluster to cluster distance is small. We also seen that small clusters result in a large osmotic pressure, so both effects seem to peak around the same point in the phase diagram. However we seen that increasing the chain length caused the number of connections per unit volume to go down and the osmotic pressure to go up. So we expect the largest value of the Flory rubber modulus is just above where the blue and orange line cross. The largest value for the osmotic pressure does not seem to have a maximum, it just keeps increasing for longer linkers. However if the linker length is to long no clusters are formed anymore and the system is no longer a gel.

5.2 Strain Stiffening

One of the most interesting effect seen is that the system can strain stiffen, this means the elastic modulus goes up if stress is exerted on the gel. We assume that both the Flory rubber theory (equation 2.43) and the osmotic pressure (equation 2.46) a play a role in the elastic modulus. In our case the binders form flowerlike micelles where coronas overlap. This overlap

gives rise to an osmotic pressure. This pressure can be related to the elastic modulus [20–22] of the system, $G_0 \sim \Pi_0$. An other effect is that these clusters are cross-linked, also giving rise

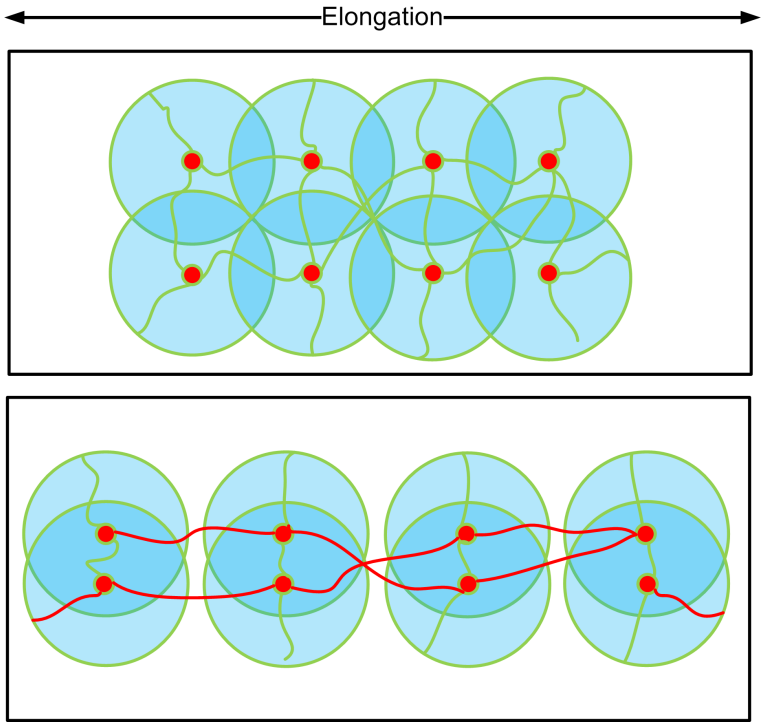

Figure 5.2: A sketch of what happens if the system is sheered. (Top) We see that the cross-links are compressed and are not contributing to the stiffness of the system. (Bottom) We see that the cores are getting spaced further apart due to the elongation and the cross-links start contribute to the stiffness.

to an finite elastic modulus [1–3]. However since in the derivation of the cross-link elasticity we started with a polymer network that was in equilibrium and ours is compressed, hence else there would be no osmotic pressure, this effect is non visible for small perturbations. For small perturbations the elastic response of the system is due to the osmotic pressure, if the system is elongated so that $L \sim L_0$ we come in the regime that represents a equilibrium polymer network and the Flory rubber elasticity kicks in. This effect is most visible for low concentrations, close to the percolation point and short chains. The concentration is because L is already closer to L_0 and only a small deformation is needed to go from one regime to the other. Where if the concentration is high, we need a large deformation meaning a large force. This large force could break the clusters internal structure destroying the cross-links and thus the elastic modulus will drop due to the gel being disintegrated. This effect will be most profound for short chains, large interaction energies and close to the percolation point.

5.3 Flower- or Rod- like Clusters

We see a different state where instead of a flowerlike motive we see an more elongated state that looks like a rod, see figure 4.4 on the right. The formation of these rods can only happen if the cluster is longer than the radius of the corona. Since we can just add a particle on the stack that is outside the radius of influence of the corona, not adding to the corona effect. If we assume we making a perfect stack of binders, the height of the cluster goes with bm where b the height of a single particle. If the cluster is the same height as the radius of gyration of the corona we are in the regime where we can just keep staking particles on the cluster. We need to solve,

$$bm = aN_0^{3/5}m^{1/5}. \tag{5.1}$$

This only has one solution for m that is larger than zero, real and non zero:

$$m \sim N_0^{3/5} \tag{5.2}$$

So, if $m > N_0^{3/5}$ (so for short chains) we find that the cluster core is larger than the corona and it becomes possible to just add more and more particles to the cluster without increasing the corona density. The theory does not cover this part of the system because for the the corona free energy equation 2.8 to be valid we need to have stay in the regime that $m < N_0^2$, meaning we are always in a flowerlike state in the model.

5.4 Technological Relevance

Last year alone there where over 8000 articles posted about physical gels in scientific journals[1] showing that physical gels are a hot topic. The reason for this is because these gels are self assembling and have a wide range of unique and controllable properties by changing the molecules they are made of. Giving them an even wider rage of applications possible, from drug delivery[11] to tissue engineering[13] and many other. The amount of material needed to make the gel is low, combining this self assembling properties makes it a cheap material to make. In this report we show that under certain conditions it is possible to predict the macroscopic properties using a free energy analysis of the microscopic building blocks. It gives insight in the dependence of the gel's macroscopic properties on the molecules the gel is made of, allowing for an optimized start for experiments and simulations saving time and money in synthesizing the desired properties of the gel.

[1] Found by searing for "Physical Gel" on http://journals.aps.org/

5.5 Future work

The theoretical part we see that the model only works in a certain regime. One limit is for sort chains this is caused by expression for corona free energy being only valid for $m \ll N_0^2$. In this regime we see rods like clusters so deriving an expression for the corona free energy for rod like systems could be useful in extending the theory. The other limit is for long chains, this is because of the cutoff function for corona effect. The function used was picked since it has the correct limits and shape but it has no good physical foundation. Having theoretical model for the corona effect would further increase the range where we can use the model.

Appendix A

Hydrogen Bonds

A.1 Dipole-Dipole Interactions

The interaction potential between two arbitrary charge distributions is given by [26]:

$$\mathcal{U}(\vec{r}_1, \vec{r}_2) = \frac{1}{4\pi\epsilon_0\epsilon_r} \int\int \frac{\rho(\vec{r}_1)\rho(\vec{r}_2)}{|\vec{r}_1 - \vec{r}_2|} \mathrm{d}^3\vec{r}_1 \mathrm{d}^3\vec{r}_2. \tag{A.1}$$

Where $\vec{r}_1$ the vector pointing to the first charge distribution and $\vec{r}_2$ to the second. When the charges do not overlap and are relatively far apart compared to there spacial distribution we can rewrite $|\vec{r}_1 - \vec{r}_2|$ [26]

$$|\vec{r}_1 - \vec{r}_2| = \left|\vec{R}_1 - (\vec{\delta}_2 + \vec{\delta}_1)\right| \tag{A.2}$$

using $\vec{R} = \vec{r}_a - \vec{r}_b$ and $\vec{r}_{1,2} = \vec{r}_{a,b} + \vec{\delta}_{1,2}$ where $\vec{\delta}$ is small. We can now make a multiple expansion around $\vec{r}_a$ and $\vec{r}_b$. Making use of the of the identities

$$q_a = \int \mathrm{d}^3\vec{r}\rho(\vec{r}_1) \tag{A.3}$$

$$\vec{\mu}_a = \int \mathrm{d}^3\vec{r}\rho(\vec{r}_1)(\vec{r}_a - \vec{\delta_1}). \tag{A.4}$$

And similar for the $\rho(\vec{r}_2)$. For the multi-pole expansion [26] we find:

$$\mathcal{U}(\vec{R}, \vec{r}_1, \vec{r}_2) = \frac{1}{4\pi\epsilon_0\epsilon_r}\left[\frac{q_a q_b}{R} + \frac{q_a\vec{\mu}_b\cdot\vec{R}}{R^3} + \frac{q_b\vec{\mu}_a\cdot\vec{R}}{R^3} + \frac{R^2\vec{\mu}_a\cdot\vec{\mu}_b - 3(\vec{\mu}_a\cdot\vec{R})(\vec{\mu}_b\cdot\vec{R})}{R^5} + ...\right]. \tag{A.5}$$

The first term is the coulomb interaction between tho charges, the second and third terms are the interaction between the dipole moment of one with the permanent charge of the other. The last term is the dipole-dipole interaction. Since our molecules do not have any net charge

the first three terms are zero, hence $q_a = q_b = 0$. The next step is to try and find and expression that does not depend on the orientation of the dipoles, $\left\langle \mathcal{U}(\vec{R}) \right\rangle$. We will do this with the help of the partition function.

$$\mathcal{Z} = \int \mathrm{d}^3 V_1 \int \mathrm{d}^3 V_2 \int \mathrm{d}^2 \vec{e}_1 \int \mathrm{d}^2 \vec{e}_2 \exp(-\beta \mathcal{U}(\vec{R}, \vec{r}_1, \vec{r}_2)). \tag{A.6}$$

We are not interested in the total partition function, but only in the part that has the rotational part of the dipoles in it. So we want some insights on the rotational dependent part of the configuration integral. By defining

$$\beta z(R) = -\ln \left(\int \mathrm{d}^2 \vec{e}_1 \int \mathrm{d}^2 \vec{e}_2 \exp(-\beta \mathcal{U}(\vec{R}, \vec{r}_1, \vec{r}_2)) \right), \tag{A.7}$$

the total partition function can be written as

$$\mathcal{Z} = \int \mathrm{d}^3 V_1 \int \mathrm{d}^3 V_2 \exp(-\beta z(R)). \tag{A.8}$$

Note that $z(R)$ is a free energy. Doing a Taylor expansion around $\beta\mathcal{U}$ and doing the integration over the angles we find that the first term is a constant and the second term is zero, the first interesting term is that with $\mathcal{U}^2$.

$$\beta z(R) = -\ln \left((4\pi)^2 + \int_0^{\pi} \frac{(\beta \mathcal{U})^2}{2} \mathrm{d}\theta_1 \sin(\theta_1) \int_0^{\pi} \mathrm{d}\theta_2 \sin(\theta_2) \int_0^{2\pi} \mathrm{d}\phi_1 \int_0^{2\pi} \mathrm{d}\phi_2 \right), \tag{A.9}$$

where

$$\mathcal{U}(\theta_1, \theta_2, \phi_1) = \frac{\mu_1 \mu_2}{4\pi\epsilon_0\epsilon_r} \frac{1}{R^3} \left[2\cos(\theta_1)\cos(\theta_2) - \sin(\theta_1)\sin(\theta_2)\cos(\phi_1) \right]. \tag{A.10}$$

Using $\ln(ab) = \ln(a) + \ln(b)$, $\ln(1+x) \approx x$ and ignoring all the constants we find the average interaction potential between two dipoles that have no net charge.

$$z(R) = -\left(\frac{\mu_1 \mu_2}{4\pi\epsilon_0\epsilon_r} \right)^2 \frac{1}{R^6} \frac{\beta}{3}. \tag{A.11}$$

A.2 Rod-Rod Interactions

The linkers can formed hydrogen bridges, these basically are dipole dipole interactions and form Appendix A.1 we know that the attractive part goes like $1/r^6$, so modeling the potential

simple Lennard-Jones potential seems like a logical step.

$$\mathcal{F}_{well}(r) = 4\epsilon \left[\left(\frac{b}{r}\right)^{12} - \left(\frac{b}{r}\right)^{6} \right], \tag{A.12}$$

where U_0 the well depth in units of k_bT and r the intermolecular distance. The point where we indefinitely destroy the gel can be calculated by looking how much work we is done by a force of exerted on the link. We model the linker as rods made up out of N individual Lennard-Jones particles with radius b that are stuck together in a rod formation. The direction of if the rod is given by the unit vector $\vec{u}_1$. We place a second rod next to the first rod. This rods orientation is given by an other unit vector $\vec{u}_2$. The two vectors $\vec{u}_1$ and $\vec{u}_2$ are $\vec{R}$ apart and make an angle θ. The vector pointing form particle n in linker one to particle m in linker

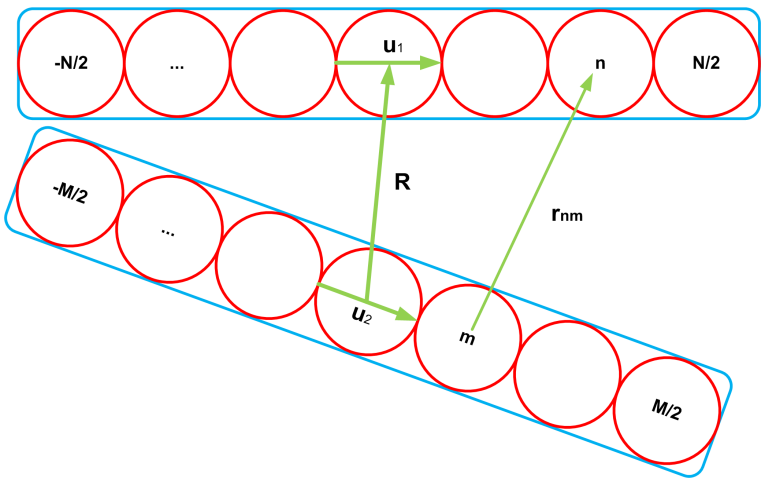

Figure A.1: Two linear Lennard-Jones rods with N interaction sides and a distance R from each other and with a relative angle θ.

two, $\vec{r}_{nm}$, is given by:

$$\vec{r}_{nm} = nb\vec{u}_1 - mb\vec{u}_2 + R, \tag{A.13}$$

$$(\vec{r}_{nm})^2 = n^2b^2 + m^2b^2 + \vec{R}^2 - 2nmb^2\vec{u}_1 \cdot \vec{u}_2. \tag{A.14}$$

The total interaction potential is given by:

$$U_{rod} = \frac{1}{2} \sum_{-N/2}^{N/2} \sum_{-N/2}^{N/2} U_{lj}\left(\vec{r}_{nm}\right), \tag{A.15}$$

where

$$\begin{aligned} U_{lj}\left(\vec{r}_{nm}\right) &= 4\epsilon\left[\left(\frac{b}{r_{nm}}\right)^{12}-\left(\frac{b}{r_{nm}}\right)^{6}\right], \\ &= U_{+}+U_{-}. \end{aligned} \tag{A.16}$$

We will now look for $m = m_*$ minimizes $\vec{r}_{nm}$ for a given n and right $\vec{r}_{nm}$ in terms of $(\vec{r}_n)_*$, where we replaced m by m_*, and some correction therm that gives the difference between $\vec{r}_{nm}$ and $(\vec{r}_n)_*$.

$$m_* = n\cos(\theta), \tag{A.17}$$

$$(\vec{r}_n)_*^2 = n^2b^2\sin^2(\theta)+\vec{R}^2, \tag{A.18}$$

$$(\vec{r}_{nm})^2 = (\vec{r}_n)_*^2+b^2\left(m-m^*\right)^2. \tag{A.19}$$

This substation enables us to replace the sum in equation A.15 by an integral and execute it analytically. We will split the integral up in two parts, one of the repulsive and one for the attractive to keep the equations readable.

$$\mathcal{U}_{-} = \frac{1}{2}\int_{-N/2}^{N/2}\mathrm{d}n\int_{-N/2}^{N/2}\mathrm{d}m\frac{4\epsilon b^6}{\left[(\vec{r}_n)_*^2+b^2\left(m-m^*\right)^2\right]^3}. \tag{A.20}$$

Substitution $x = b(m - m_*)$ and $y = nb\sin(\theta)$.

$$U_{-} = -\frac{2\epsilon b^4}{\sin(\theta)}\int_{-a}^{a}\mathrm{d}n\int_{-b}^{b}\mathrm{d}m\left[x^2+y^2+\vec{R}^2\right]^{-3}, \tag{A.21}$$

where $a = \frac{N}{2}\sin(\theta)$ and $b = \frac{N}{2}+\frac{x}{\tan(\theta)}$. If $N \gg b$, so the rod is a lot longer than the distance from the center of the rod to the minimum in the interaction potential and $\theta \leq b/N$ so the angle is small and making use that the function decays fast for large values of x and y we can replace the integration boundaries to go from ∞ to $-\infty$ resulting in:

$$U_{-} = -\frac{\epsilon\pi b^4}{R^4\sin(\theta)}. \tag{A.22}$$

Very similar we can calculate U_+ resulting in:

$$U = 4\epsilon\left[\frac{\pi}{10}\left(\frac{b}{R}\right)^{10}-\frac{\pi}{4}\left(\frac{b}{R}\right)^{4}\right]\frac{1}{\sin(\theta)}, \tag{A.23}$$

approximating $\theta \approx b/l$ and making a Taylor expansion around zero we find:

$$U \approx \frac{4\epsilon L}{b}\left[\frac{\pi}{10}\left(\frac{b}{R}\right)^{10} - \frac{\pi}{4}\left(\frac{b}{R}\right)^{4}\right], \tag{A.24}$$

where $\epsilon L \approx n\epsilon b$ making the interaction energy between two Lennard-Jones rods with a number of n bonding sites

$$U \approx 4(\epsilon \times n)\left[\frac{\pi}{10}\left(\frac{b}{R}\right)^{10} - \frac{\pi}{4}\left(\frac{b}{R}\right)^{4}\right]. \tag{A.25}$$

The minimum in the energy is at $R = b$ and thus:

$$U_{min} = -\frac{3(\epsilon \times n)\pi}{5}. \tag{A.26}$$

Appendix B

Polymer Chain Entropy

B.1 Statistics of a Gaussian chain

The freely joined chain is a model for long polymer molecules. The model uses a coarse grained view of the molecule where we make that the direction vector along the polymer becomes uncorrelated over long distances. This assumption results in that there is no energetic penalty for bending the chain. This is why the model is also referred to as ideal chain or Gaussian chain. The probability on finding an end to end distance of this type for the chain is given by:

$$\mathcal{P}(\vec{R}) = \left\langle \delta\left(\vec{R} - \sum_{i=1}^{N} \vec{r}_i\right)\right\rangle. \tag{B.1}$$

The probability of finding a chain with length R is 1 if the chain has this length and is zero if it doesn't. Using the integral representation of the Dirac delta found via residue calculus,

$$\delta(x-n) = \frac{1}{2\pi i}\oint_{|z|=1} z^{x-n-1}\mathrm{d}z = \frac{1}{2\pi}\int_0^{2\pi} e^{i(x-n)\phi}\mathrm{d}\phi. \tag{B.2}$$

The probability of finding a end to end distance of $\vec{R}$ is equal to:

$$\mathcal{P}(\vec{R}) = \frac{1}{(2\pi)^3}\left\langle \int \mathrm{d}^3k \exp\left(i\vec{k}\cdot\left[\vec{R} - \sum_{i=1}^{N}\vec{r}_i\right]\right)\right\rangle. \tag{B.3}$$

Now we can make use of the fact that all the probabilities for for finding a vector $\vec{r}_i$ are independent; the average of the product of the probabilities is the same as the product of the probabilities $\langle r_1 r_2\rangle = \langle r_1\rangle\langle r_2\rangle$.

$$\mathcal{P}(\vec{R}) = \prod_{i=1}^{N}\int \mathrm{d}^3 r_i P(\vec{r}_i)\left\{\frac{1}{(2\pi)^3}\int \mathrm{d}^3k \exp\left(i\vec{k}\cdot\left[\vec{R}-\vec{r}_i\right]\right)\right\} \tag{B.4}$$

We also know that all the parts of the chain are identical so $P(\vec{r}_i)$, so the product factorizes.

$$\mathcal{P}(\vec{R}) = \frac{1}{(2\pi)^3}\int \mathrm{d}^3k \exp\left(i\vec{k}\cdot\vec{R}\right)\left[\int \mathrm{d}^3k P(\vec{r})\exp\left(-i\vec{k}\cdot\vec{r}\right)\right]^N \tag{B.5}$$

$P(\vec{(}r)$ has its mean value at zero and finite second moment, the Fourier transform of will have its maximum around $k = 0$ and go to zero for large values of k. Raising such a function to the Nth power leaves us with a function that differs from zero only very close to the origin, and which may be approximated by:

$$\begin{aligned}\left[\int \mathrm{d}^3k P(\vec{r})\exp\left(-i\vec{k}\cdot\vec{r}\right)\right]^N &\approx \left[1-\frac{1}{2}\left\langle\left(\vec{k}\cdot\vec{r}\right)^2\right\rangle\right]^N \\ &\approx 1-\frac{N}{2}\left\langle\left(\vec{k}\cdot\vec{r}\right)^2\right\rangle + \mathcal{O}(r^4) \\ &= 1-\frac{N}{6}k^2\left\langle\vec{r}^2\right\rangle + \mathcal{O}(r^4) \\ &\approx e^{-\frac{1}{6}Nk^2\left\langle\vec{r}^2\right\rangle}\end{aligned} \tag{B.6}$$

Using this result and substituting it back in toB.5. Making use of symmetry, $P(r) = P_x(r_x)P_y(r_y)P_z(r_z)$ we have to solve the $1D$ probability integrals. Doing this we find our end to end distance probability:

$$\mathcal{P}(\vec{R}) = \left(\frac{3}{2\pi N\left\langle\vec{r}^2\right\rangle}\right)^{\frac{3}{2}}\exp\left(-\frac{3R^2}{2N\left\langle\vec{r}^2\right\rangle}\right) \tag{B.7}$$

B.2 Free Energy of a Self Avoiding Polymer

The interaction between the monomers is given by a potential that only depends on the distance between the two monomers, $\mathcal{U}(|\vec{r}|)$. Since our chains are still modeled as being ideal we can model them as an ideal "gas" of lose monomers in a box of size V. The free energy cost of putting N monomers with volume v in a box of volume V goes as: $v(N/V)\times V$. The probability it runs into an other polymer goes with N/V. The typical energy scale is thermal, k_bT, so we get [27],

$$\Delta\mathcal{F}_{avoid} \approx \frac{v\mathrm{k_b}TN_0^2}{V}. \tag{B.8}$$

Where we pick $V = R^3$. Now if the concentration of polymers is high we expect them to become longer then they would in the case of a diluted system, this causes the entropy cost to rise:

$$\Delta\mathcal{F}_{ideal} \approx \frac{3\mathrm{k_b}TR^2}{2N_0a^2}. \tag{B.9}$$

Using this we can calculate the distribution function of R,

$$P(R) = \frac{1}{\mathcal{Z}} e^{-\beta(\Delta\mathcal{F}_i + \Delta\mathcal{F}_a)}, \tag{B.10}$$

and from this we can find $\langle R \rangle$, unfortunately we cannot execute the integral analytically. However we know that the function $e^{-f(x)}$ is strongly peaked around the minimum value of $f(x)$ so we approximate the exponent by a Kronecker delta on x_{min} (saddle point approximation):

$$\begin{aligned} \langle x \rangle &\sim \int x e^{-f(x)} \mathrm{d}x, \\ &\approx \int x \delta(x - x_{min}) \mathrm{d}x, \\ &= x_{min}. \end{aligned} \tag{B.11}$$

So we only need minimize $\Delta\mathcal{F}_i + \Delta\mathcal{F}_a$ with respect to R,

$$\langle R \rangle \sim N_0^{3/5}. \tag{B.12}$$

And the extra free energy cost associated with the ideal self avoiding chain:

$$\Delta\mathcal{F}_{avoid} \sim k_b N_0^{1/5}. \tag{B.13}$$

B.3 Entropy of an Extended Chain

If we start with z loose binders, where every binder has one linker and we make a chain extended system for these lose units the entropy is changed. From expression B.7 that the that the entropy of a Gaussian depends on R, the end to end distance and N the number of monomers and is given by[18]:

$$S(R) = \frac{3k_b}{2} \log\left(\frac{3}{2\pi N a^2}\right) - \frac{3\mathrm{k_b}\vec{R}^2}{2Na^2}. \tag{B.14}$$

he entropy difference concerning the Gaussian chains is if the bonds are formed the link-chain goes from z lose units with N_0 monomers to one long chain with $N = zN_0$ monomers. To make this calculation possible we will set the end to end distance to be zero, this is (almost)

true for a loop. This cost entropy of folding up the linker-chain:

$$\begin{aligned}
\Delta S &= \frac{3k_b}{2}\log\left(\frac{3}{2\pi N_0 z a^2}\right) - \frac{3zk_b}{2}\log\left(\frac{3}{2\pi N_0 a^2}\right), \\
&= -\frac{3k_b}{2}\left((z-1)\log\left(\frac{3}{2\pi N_0 a^2}\right) + \log(z)\right), \\
&= -\lim_{z\to\infty}\frac{3(z-1)k_b}{2}\left(\log\left(\frac{3}{2\pi N_0 a^2}\right) + \frac{\log(z)}{z-1}\right), \\
&= -\frac{3zk_b}{2}\log\left(\frac{3}{2\pi N_0 a^2}\right).
\end{aligned} \tag{B.15}$$

B.4 Entropy of Folding the Chain

To find the entropy difference between the free and stacked state we use the same notation as we did as in equation B.1 and write the term in the Dirac delta in terms of the individual linkers under to constrain that the sum of the end to end distances of the parts is equal to that of the long chain.

$$\begin{aligned}
\mathcal{P}(\vec{R}) &= \left\langle \delta\left(\vec{R} - \sum_{i=1}^{N}\vec{r}_i\right)\right\rangle \\
&= \left\langle \delta\left(\sum_{j=1}^{m}\vec{R}_j - \sum_{j=1}^{m}\sum_{i=1}^{N}\vec{r}_i\right)\right\rangle \\
&\approx \prod_{j=1}^{m}\left\langle \delta\left(\vec{R}_j - \sum_{i=1}^{N}\vec{r}_i\right)\right\rangle \\
&\approx \left(\mathcal{P}(\vec{R}_j)\right)^m.
\end{aligned} \tag{B.16}$$

So along as all the individual chains are the same and can be handled as Gaussian we will see no entropy difference for the chains themselves between the stacked and the unstacked state.

When we look to the system as a whole we see that forming the cluster we lose configuration entropy. In a system with $\mathcal{Z}$ unlinked particles we have $\Omega = \mathcal{Z}!$ unique permutations and $\mathcal{Z}$ particles. If clusters are formed we are left with $(\mathcal{Z}!/\prod m_i!)$ unique permutations, where m_i the size of the i-th subsystem. The entropy change per particle,

$$\begin{aligned}
\Delta S_{config,1} &= k_b\left[\ln\left(\frac{\mathcal{Z}!}{\prod m_i!}\right) - \ln(\mathcal{Z}!)\right], \\
&= -k_b\ln\left(\prod m_i!\right), \\
&= -\frac{\mathcal{Z}k_b\ln(m_i!)}{m}.
\end{aligned} \tag{B.17}$$

The subsystem itself used also loses all its internal permutations because the particles are

fixed relative to another if a bond is formed, the entropic loss due to this is given by:

$$\begin{aligned} \Delta S_{config,2} &= k_b \left[m \ln(1!) - \ln(m!) \right], \\ &= -k_b \ln\left(m!\right), \end{aligned} \tag{B.18}$$

per cluster.

References

[1] Paulina J. Skrzeszewska, Frits A. de Wolf, Martien A. Cohen Stuarta, and Jasper van der Gucht. Kinetics of network formation by telechelic polypeptides with trimeric nodes. *Soft Matter*, 6:416–422, 2010. ii, 44

[2] Paulina J. Skrzeszewska, Joris Sprakel, Frits A. de Wolf, Remco Fokkink, Martien A. Cohen Stuart, and Jasper van der Gucht. Fracture and self-healing in a well-defined self-assembled polymer network. *Macromolecules*, 43:2542–3548, 2010.

[3] Helena Teles, Paulina J. Skrzeszewska, Marc W. T. Werten, Jasper van der Gucht, Gerrit Egginkab, and Frits A. de Wolf. Influence of molecular size on gel-forming properties of telechelic collageninspired polymers. *Soft Matter*, 6:4681–4687, 2010. ii, 44

[4] International Union of Pure, Applied Chemistry. Commission on Macromolecular Nomenclature, and R.G. Jones. *Compendium of Polymer Terminology and Nomenclature: IUPAC Recommendations, 2008.* IUPAC Chemical Nomenclature Series. RSC Pub., 2009. 1

[5] M. Rubinstein and R.H. Colby. *Polymer Physics.* OUP Oxford, 2003. 1, 18, 20

[6] Min Wang, Ling Xu, Jing Peng, Maolin Zhai, Jiuqiang Li, and Genshuan Wei. Adsorption and desorption of sr(ii) ions in the gels based on polysaccharide derivates. *Journal of Hazardous Materials*, 171(13):820 – 826, 2009. 1

[7] Baljit Singh and S. Kumar. Synthesis and characterization of psyllium-nvp based drug delivery system through radiation crosslinking polymerization. *Nuclear Instruments and Methods in Physics Research Section B: Beam Interactions with Materials and Atoms*, 266(15):3417 – 3430, 2008. 1

[8] Tianhong Chen, Heather D. Embree, Li-Qun Wu, and Gregory F. Payne. In vitro protein-polysaccharide conjugation: Tyrosinase-catalyzed conjugation of gelatin and chitosan. *Biopolymers*, 64(6):292–302, 2002. 1

[9] Wei Shen, Julia A. Kornfield, and David A. Tirrell. Structure and mechanical properties

of artificial protein hydrogels assembled through aggregation of leucine zipper peptide domains. *Soft Matter*, 3:99–107, 2007. 2

[10] Sang Cheon Lee., Yong Woo Cho, and Kinam Park. Control of thermogelation properties of hydrophobically-modified methylcellulose. *Journal of Bioactive and Compatible Polymers*, 20:5–13, 2005. 2

[11] Marc Sutter, Juergen Siepmann, Wim E. Hennink, and Wim Jiskoot. Recombinant gelatin hydrogels for the sustained release of proteins. *Journal of Controlled Release*, 119(3):301 – 312, 2007. 2, 45

[12] Biji Balakrishnan, M. Mohanty, P.R. Umashankar, and A. Jayakrishnan. Evaluation of an in situ forming hydrogel wound dressing based on oxidized alginate and gelatin. *Biomaterials*, 26(32):6335 – 6342, 2005. 2

[13] Byung-Soo Kim and David J Mooney. Development of biocompatible synthetic extracellular matrices for tissue engineering. *Trends in Biotechnology*, 16(5):224 – 230, 1998. 2, 45

[14] G.O. Phillips, S. Al-Assaf, P.A. Williams, A. du Plessis, and C.J. Yim. Radiation demineralised bone enhanced osteoinductive capacity after transplantation. *Nuclear Instruments and Methods in Physics Research Section B: Beam Interactions with Materials and Atoms*, 265(1):390 – 393, 2007. 2

[15] Yan Han, Qiongyu Zeng, Haiyan Li, and Jiang Chang. The calcium silicate/alginate composite: Preparation and evaluation of its behavior as bioactive injectable hydrogels. *Acta Biomaterialia*, 9(11):9107 – 9117, 2013. 2

[16] Jungahn Kim, Sang Seob Kim, Keon Hyeong Kim, Yong Hyun Jin, Soon Man Hong, Seung San Hwang, Bong-Gyoo Cho, Dong Youn Shin, and Seung Soon Im. Applications of telechelic polymers as compatibilizers and stabilizers in polymer blends and inorganic/organic nanohybrids. *Polymer*, 45(10):3527 – 3533, 2004. 2

[17] A. N. Semenov and Michael Rubinstein. Dynamics of entangled associating polymers with large aggregates. *Macromolecules*, 35(12):4821–4837, 2002. 8

[18] P. J. Flory. *Principles of polymer chemistry*. Cornell University Press, 1953. 8, 16, 17, 55

[19] L.C.Case. Branching polymers i. network defects. *J. Polym. Sci*, 1960. 14

[20] Giovanni Romeo and Massimo Pica Ciamarra. Elasticity of compressed microgel suspensions. *Soft Matter*, 9:5401–5406, 2013. 20, 44

[21] T. G. Mason, J. Bibette, and D. A. Weitz. Elasticity of compressed emulsions. *Phys. Rev. Lett.*, 75:2051–2054, Sep 1995.

[22] Juan José Liétor-Santos, Benjamín Sierra-Martín, and Alberto Fernández-Nieves. Bulk and shear moduli of compressed microgel suspensions. *Phys. Rev. E*, 84:060402, Dec 2011. 20, 44

[23] S. Alexander. Adsorption of chain molecules with a polar head a scaling description. *J. Phys. (France)*, 38(8):983–987, 1977. 20

[24] P.G. de Gennes. Polymers at an interface; a simplified view. *Advances in Colloid and Interface Science*, 27(34):189 – 209, 1987. 20

[25] Virginie Hugouvieux, Monique A. V. Axelos, and Max Kolb. Micelle formation, gelation and phase separation of amphiphilic multiblock copolymers[dagger]. *Soft Matter*, 7:2580–2591, 2011. 31

[26] David J. Griffiths. *Introduction to Electrodynamics (3rd Edition)*. Benjamin Cummings, 1998. 47

[27] R.A.L. Jones. *Soft Condensed Matter*. Oxford Master Series in Physics. OUP Oxford, 2002. 54